

# Extra-Large G Proteins Expand the Repertoire of Subunits in Arabidopsis Heterotrimeric G Protein Signaling<sup>1[OPEN]</sup>

David Chakravorty<sup>2</sup>, Timothy E. Gookin<sup>2</sup>, Matthew J. Milner<sup>3</sup>, Yunqing Yu, and Sarah M. Assmann\*

Biology Department, Pennsylvania State University, University Park, Pennsylvania 16802

ORCID IDs: 0000-0002-6591-4853 (D.C.); 0000-0002-0994-0790 (T.E.G.); 0000-0001-9184-7423 (M.J.M.); 0000-0003-4541-1594 (S.M.A.).

Heterotrimeric G proteins, consisting of  $G\alpha$ ,  $G\beta$ , and  $G\gamma$  subunits, are a conserved signal transduction mechanism in eukaryotes. However, G protein subunit numbers in diploid plant genomes are greatly reduced as compared with animals and do not correlate with the diversity of functions and phenotypes in which heterotrimeric G proteins have been implicated. In addition to GPA1, the sole canonical Arabidopsis (*Arabidopsis thaliana*)  $G\alpha$  subunit, Arabidopsis has three related proteins: the extra-large GTP-binding proteins XLG1, XLG2, and XLG3. We demonstrate that the XLGs can bind  $G\beta\gamma$  dimers (AGB1 plus a  $G\gamma$  subunit: AGG1, AGG2, or AGG3) with differing specificity in yeast (*Saccharomyces cerevisiae*) three-hybrid assays. Our in silico structural analysis shows that XLG3 aligns closely to the crystal structure of GPA1, and XLG3 also competes with GPA1 for  $G\beta\gamma$  binding in yeast. We observed interaction of the XLGs with all three  $G\beta\gamma$  dimers at the plasma membrane in planta by bimolecular fluorescence complementation. Bioinformatic and localization studies identified and confirmed nuclear localization signals in XLG2 and XLG3 and a nuclear export signal in XLG3, which may facilitate intracellular shuttling. We found that tunicamycin, salt, and glucose hypersensitivity and increased stomatal density are *agb1*-specific phenotypes that are not observed in *gpa1* mutants but are recapitulated in *xlg* mutants. Thus, XLG- $G\beta\gamma$  heterotrimers provide additional signaling modalities for tuning plant G protein responses and increase the repertoire of G protein heterotrimer combinations from three to 12. The potential for signal partitioning and competition between the XLGs and GPA1 is a new paradigm for plant-specific cell signaling.

The classical heterotrimeric G protein consists of a GDP/GTP-binding  $G\alpha$  subunit with GTPase activity bound to an obligate dimer formed by  $G\beta$  and  $G\gamma$  subunits. In the signaling paradigm largely elucidated from mammalian systems, the plasma membrane-associated heterotrimer contains  $G\alpha$  in its GDP-bound form. Upon receiving a molecular signal, typically transduced by a transmembrane protein (e.g. a G protein-coupled receptor),  $G\alpha$  exchanges GDP for GTP and dissociates from the  $G\beta\gamma$  dimer. Both  $G\alpha$  and  $G\beta\gamma$  interact with intracellular effectors to initiate downstream signaling cascades. The intrinsic GTPase activity of  $G\alpha$  restores  $G\alpha$  to the GDP-bound form, which binds  $G\beta\gamma$ ,

thereby reconstituting the heterotrimer (McCudden et al., 2005; Oldham and Hamm, 2008).

Signal transduction through a heterotrimeric G protein complex is an evolutionarily conserved eukaryotic mechanism common to metazoa and plants, although there are distinct differences in the functional intricacies between the evolutionary branches (Jones et al., 2011a, 2011b; Bradford et al., 2013). The numbers of each subunit encoded within genomes, and therefore the potential for combinatorial complexity within the heterotrimer, is one of the most striking differences between plants and animals. For example, the human genome encodes 23  $G\alpha$  (encoded by 16 genes), five  $G\beta$ , and 12  $G\gamma$  subunits (Hurowitz et al., 2000; McCudden et al., 2005; Birnbaumer, 2007). The Arabidopsis (*Arabidopsis thaliana*) genome, however, only encodes one canonical  $G\alpha$  (GPA1; Ma et al., 1990), one  $G\beta$  (AGB1; Weiss et al., 1994), and three  $G\gamma$  (AGG1, AGG2, and AGG3) subunits (Mason and Botella, 2000, 2001; Chakravorty et al., 2011), while the rice (*Oryza sativa*) genome encodes one  $G\alpha$  (Ishikawa et al., 1995), one  $G\beta$  (Ishikawa et al., 1996), and either four or five  $G\gamma$  subunits (Kato et al., 2004; Chakravorty et al., 2011; Botella, 2012). As expected, genomes of polyploid plants have more copies due to genome duplication, with the soybean (*Glycine max*) genome encoding four  $G\alpha$ , four  $G\beta$  (Bisht et al., 2011), and 10  $G\gamma$  subunits (Choudhury et al., 2011). However, Arabidopsis heterotrimeric G proteins have been implicated in a surprisingly large number of phenotypes, which is seemingly contradictory given the relative scarcity of subunits. Arabidopsis G proteins have been implicated in cell division (Ullah

<sup>1</sup> This work was supported by the National Science Foundation (grant no. MCB-1121612 to S.M.A.) and by the U.S. Department of Agriculture/Agriculture and Food Research Initiative (postdoctoral grant no. 2011-67012-30722 to M.J.M.).

<sup>2</sup> These authors contributed equally to the article.

<sup>3</sup> Present address: John Bingham Laboratory, National Institute for Agricultural Botany, Cambridge CB3 0LE, UK.

\* Address correspondence to sma3@psu.edu.

The author responsible for distribution of materials integral to the findings presented in this article in accordance with the policy described in the Instructions for Authors ([www.plantphysiol.org](http://www.plantphysiol.org)) is: Sarah M. Assmann (sma3@psu.edu).

D.C. and T.E.G. performed the majority of the research; M.J.M. and Y.Y. performed additional experiments; S.M.A. supervised the research; D.C., T.E.G., and S.M.A. wrote the article with contributions from all authors.

[OPEN] Articles can be viewed without a subscription.

[www.plantphysiol.org/cgi/doi/10.1104/pp.15.00251](http://www.plantphysiol.org/cgi/doi/10.1104/pp.15.00251)

et al., 2001; Chen et al., 2006) and morphological development in various tissues, including hypocotyls (Ullah et al., 2001, 2003), roots (Ullah et al., 2003; Chen et al., 2006; Li et al., 2012), leaves (Lease et al., 2001; Ullah et al., 2001), inflorescences (Ullah et al., 2003), and flowers and siliques (Lease et al., 2001), as well as in pathogen responses (Llorente et al., 2005; Trusov et al., 2006; Cheng et al., 2015), regulation of stomatal movement (Wang et al., 2001; Coursol et al., 2003; Fan et al., 2008) and development (Zhang et al., 2008; Nilson and Assmann, 2010), cell wall composition (Delgado-Cerezo et al., 2012), responses to various light stimuli (Warpeha et al., 2007; Botto et al., 2009), responses to multiple abiotic stimuli (Huang et al., 2006; Pandey et al., 2006; Trusov et al., 2007; Zhang et al., 2008; Colaneri et al., 2014), responses to various hormones during germination (Ullah et al., 2002), and postgermination development (Ullah et al., 2002; Pandey et al., 2006; Trusov et al., 2007). Since the  $G\gamma$  subunit appeared to be the only subunit that provides diversity in heterotrimer composition in Arabidopsis, it was proposed that all functional specificity in heterotrimeric G protein signaling was provided by the  $G\gamma$  subunit (Trusov et al., 2007; Chakravorty et al., 2011; Thung et al., 2012, 2013). This allowed for only three heterotrimer combinations to account for the wide range of G protein-associated phenotypes.

In addition to the above typical G protein subunits, the plant kingdom contains a conserved protein family of extra-large GTP-binding proteins (XLGs). XLGs differ from typical  $G\alpha$  subunits in that they possess a long N-terminal extension of unknown function, but they are similar in that they all have a typical C-terminal  $G\alpha$ -like region, with five semiconserved G-box (G1–G5) motifs. The XLGs also possess the two sequence features that differentiate heterotrimeric G protein  $G\alpha$  subunits from monomeric G proteins: a helical region between the G1 and G2 motifs and an Asp/Glu-rich loop between the G3 and G4 motifs (Lee and Assmann, 1999; Ding et al., 2008; Heo et al., 2012). The Arabidopsis XLG family comprises XLG1, XLG2, and XLG3, and all three have demonstrated GTP-binding and GTPase activities, although they differ from GPA1 in exhibiting a much slower rate of GTP hydrolysis, with a  $Ca^{2+}$  cofactor requirement instead of an  $Mg^{2+}$  requirement, as for canonical  $G\alpha$  proteins (Heo et al., 2012). All three Arabidopsis XLGs were observed to be nuclear localized (Ding et al., 2008). Although much less is known about XLGs than canonical  $G\alpha$  subunits, XLG2 positively regulates resistance to the bacterial pathogen *Pseudomonas syringae* and was immunoprecipitated with AGB1 from tissue infected with *P. syringae* (Zhu et al., 2009). *xlg3* mutants, like *agb1* mutants, are impaired in root-waving and root-skewing responses (Pandey et al., 2008). During the preparation of this report, Maruta et al. (2015) further investigated XLG2, particularly focusing on the link between XLG2 and  $G\beta\gamma$  in pathogen responses. Based on symptom progression in *xlg* mutants, they found that XLG2 is a positive regulator of resistance to both bacterial and

fungal pathogens, with a minor contribution from XLG3 in resistance to *Fusarium oxysporum*. XLG2 and XLG3 are also positive regulators of reactive oxygen species (ROS) production in response to pathogen-associated molecular pattern elicitors. The resistance and pathogen-associated molecular pattern-induced ROS phenotypes of the *agg1 agg2* and *xlg2 xlg3* double mutants were not additive in an *agg1 agg2 xlg2 xlg3* quadruple mutant, indicating that these two XLGs and the two  $G\gamma$  subunits function in the same, rather than parallel, pathways. Unfortunately, the close proximity of XLG2 and AGB1 on chromosome 4 precluded the generation of an *agb1 xlg2* double mutant; therefore, direct genetic evidence of XLG2 and AGB1 interaction is still lacking, but physical interactions between XLG2 and the  $G\beta\gamma$  dimers were shown by yeast (*Saccharomyces cerevisiae*) three-hybrid and bimolecular fluorescence complementation (BiFC) assays (Maruta et al., 2015). Localization of all three XLGs was also reexamined, indicating that XLGs are capable of localizing to the plasma membrane in addition to the nucleus (Maruta et al., 2015).

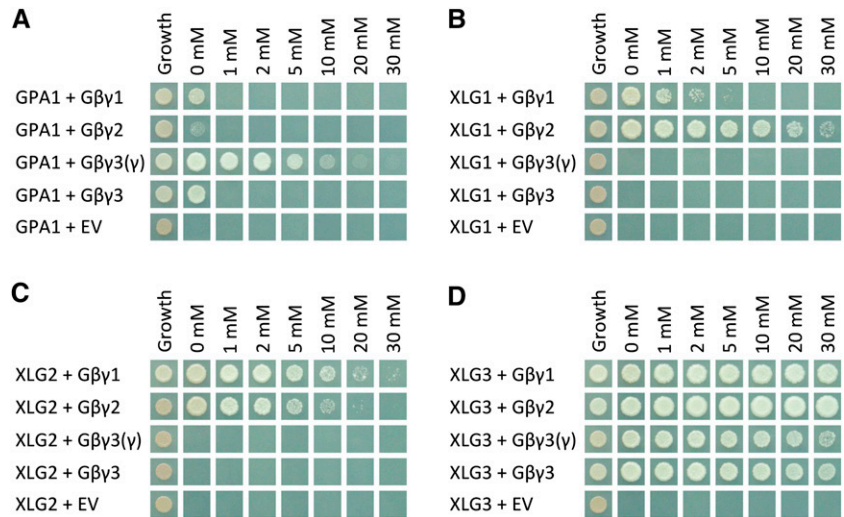
Interestingly, several other plant G protein-related phenotypes, in addition to pathogen resistance, have been observed only in  $G\beta$  and  $G\gamma$  mutants, with opposite phenotypes observed in  $G\alpha$  (*gpa1*) mutants. Traditionally, the observation of opposite phenotypes in  $G\alpha$  versus  $G\beta\gamma$  mutants in plants and other organisms has mechanistically been attributed to signaling mediated by free  $G\beta\gamma$ , which increases in abundance in the absence of  $G\alpha$ . However, an intriguing alternative is that XLG proteins fulfill a  $G\alpha$ -like role in forming heterotrimeric complexes with  $G\beta\gamma$  and function in non-GPA1-based G protein signaling processes. If XLGs function like  $G\alpha$  subunits, the corresponding increase in subunit diversity could potentially account for the diversity of G protein phenotypes. In light of this possibility, we assessed the heterotrimerization potential of all possible XLG and  $G\beta\gamma$  dimer combinations, XLG localization and its regulation by  $G\beta\gamma$ , and the effect of *xlg* mutation on selected known phenotypes associated with heterotrimeric G proteins. Our results provide compelling evidence for the formation of XLG- $G\beta\gamma$  heterotrimers and reveal that plant G protein signaling is substantially more complex than previously thought.

## RESULTS

### XLG- $G\beta\gamma$ Interaction in Vivo

Maruta et al. (2015) previously reported that XLG2 interacts with AGB1/AGG1, AGB1/AGG2, and AGB1/AGG3 in yeast three-hybrid assays, but they did not test the ability of XLG1 or XLG3 to interact with any of the  $G\beta\gamma$  dimers. We tested all three XLGs against all three  $G\beta\gamma$  dimers. Evidence for a transmembrane domain in AGG3, which would place the C terminus of AGG3 outside of the cell (Wolfenstetter et al., 2015), was taken into consideration by including an additional AGB1/AGG3 construct [designated  $G\beta\gamma3(\gamma)$ ], in which

**Figure 1.** Yeast three-hybrid assays demonstrate the specificity of GPA1 for AGB1/AGG3, XLG1 and XLG2 for AGB1/AGG1 and AGB1/AGG2, and XLG3 for all three  $G\beta\gamma$  dimers. Yeast three-hybrid assays tested the interactions between GPA1 (A), XLG1 (B), XLG2 (C), and XLG3 (D; GAL4 activation domain fusions) with the AGB1/AGG1 ( $G\beta\gamma1$ ), AGB1/AGG2 ( $G\beta\gamma2$ ), and AGB1/AGG3 ( $G\beta\gamma3$ )  $G\beta\gamma$  dimers ( $G\gamma$  fused to the GAL4 binding domain, with  $G\beta$  [AGB1] as the bridge protein). A truncated  $\gamma3(\gamma)$  was also tested, consisting of only the  $G\gamma$ -like domain of AGG3 (residues 1–112), lacking the implicated transmembrane domain. Yeast growth on synthetic complete (SC)-Trp-Leu confirmed transformation and cell viability. Interactions were assayed on SC-Trp-Leu-Met-His supplemented with the indicated concentrations of 3-AT (0–30 mM). EV, Empty vector.



only the  $G\gamma$ -like domain (residues 1–112) of AGG3 was fused to the GAL4 binding domain. We also investigated interaction strength within the complexes, wherein growth on higher concentrations of 3-amino-1,2,4-triazole (3-AT) is an accepted indicator of a stronger or more stable interaction (Durfee et al., 1993; Ursic et al., 2004).

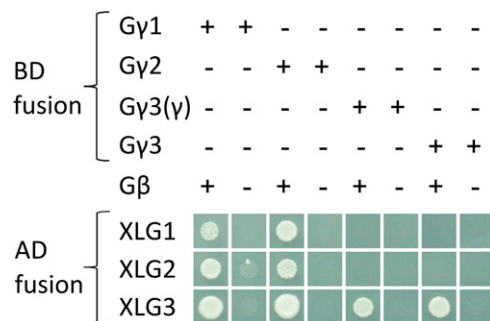
The interaction between GPA1 and  $G\beta\gamma$  dimers containing AGG1 or AGG2 was quite weak, with yeast growth observed only in the absence of 3-AT. The only dimer with which GPA1 showed a strong interaction was AGB1/AGG3( $\gamma$ ) (Fig. 1A). XLG1 and XLG2 interaction with  $G\beta\gamma$  dimers containing AGG1 or AGG2 (Fig. 1, B and C) was stronger than that of GPA1. XLG1 and XLG2 did not interact in yeast with  $G\beta\gamma$  dimers containing AGG3 (Fig. 1, B and C); however, XLG3 interacted strongly with all  $G\beta\gamma$  dimers, including those containing AGG3 (Fig. 1D). Therefore, we found strong evidence from this approach for the interaction of eight of the 12 heterotrimeric complexes tested.

In the above assays, the XLGs or GPA1 were fused to the GAL4 activation domain, the  $G\gamma$  subunits (AGG1, AGG2, or AGG3) were fused to the GAL4 binding domain (multiple cloning site 1 [MCS1] of the yeast three-hybrid vector pBridge), and AGB1 was used as the bridge protein, expressed from MCS2 of pBridge. Therefore, it was possible that the yeast reporter genes were activated by direct interaction between each XLG and each  $G\gamma$  subunit. To assess whether the yeast three-hybrid interactions do in fact involve a heterotrimeric interaction (i.e. with a requirement for AGB1), the AGB1 bridge protein was not included, and the assay was repeated. As shown in Figure 2, coexpression of the  $G\beta$  subunit, AGB1, was required for interaction. These results raised the hypothesis that GPA1 and the XLGs may compete with each other for  $G\beta\gamma$  binding. Since XLG1 and XLG2 did not bind the same  $G\beta\gamma$  dimers as GPA1 in yeast (Fig. 1), XLG3 and AGB1/AGG3( $\gamma$ ) were selected to test this hypothesis. Either GPA1 or XLG3 was expressed under the control of the strong





*GPD* promoter (Bitter and Egan, 1984; Partow et al., 2010), in competition with the GAL4:XLG3 or GAL4:GPA1 activation domain fusion, respectively. XLG3 was able to inhibit GPA1-AGB1/AGG3 interaction, and GPA1 was able to inhibit XLG3-AGB1/AGG3 interaction (Fig. 3).

### XLG Three-Dimensional Structure Analysis in Silico

The ability of all three XLGs to interact with  $G\beta\gamma$  dimers, and of XLG3 to compete with GPA1 in yeast, suggests that all four G proteins are structurally similar. As seen in the alignment of Ding et al. (2008), primary sequence conservation between GPA1 and the XLG proteins is moderate, with percentage identities of GPA1 and the XLG  $G\alpha$  domains of 26.1%, 23.2%, and



**Figure 2.** The interaction of XLGs with  $G\gamma$  subunits is AGB1 dependent. Yeast three-hybrid assays tested the interactions of GPA1, XLG1, XLG2, and XLG3 with the AGG1 ( $G\gamma1$ ), AGG2 ( $G\gamma2$ ), and AGG3 ( $G\gamma3$ ) subunits. Interactions were assayed in the presence and absence of AGB1. A truncated  $\gamma3(\gamma)$  subunit was also included, which includes only the  $G\gamma$ -like domain of AGG3 (residues 1–112). All interactions were assayed by growth on SC-Trp-Leu-Met-His supplemented with 2 mM 3-AT. Two millimolars of 3-AT was used because the pBridge-AGG1 construct exhibited autoactivation (i.e. growth in combination with the empty vector) on SC-Trp-Leu-Met-His supplemented with 0 or 1 mM 3-AT.

AD fusion	GPA1	+	+	-	-
	XLG3	-	-	+	+
GPD pr	GPA1	-	-	-	+
	XLG3	-	+	-	-
BD fusion	Gβγ3(γ)				

**Figure 3.** GPA1 and XLG3 compete with each other for binding of AGB1/AGG3 in yeast. Yeast three-hybrid competition assays tested the interaction between GPA1 and AGB1/AGG3(γ) [Gβγ3(γ)] with or without additional expression of XLG3 and the interaction between XLG3 and AGB1/AGG3(γ) [Gβγ3(γ)] with or without additional expression of GPA1. The fourth protein (XLG3 or GPA1, respectively) was expressed under the control of the strong GPD promoter (pr). All interactions were assayed by growth on SC-Trp-Leu-Met-His supplemented with 2 mM 3-AT.

28.5% for XLG1<sup>446-888</sup>, XLG2<sup>435-861</sup>, and XLG3<sup>396-848</sup>, respectively. Therefore, we performed an *in silico* analysis of each XLG using Phyre<sup>2</sup> (Kelley and Sternberg, 2009), which generates a protein fold profile for subsequent analysis by the secondary structure predictor Psi-Pred (Jones, 1999b). Phyre<sup>2</sup> then identifies similar tertiary structures in a fold library via profile-profile alignments (Kelley and Sternberg, 2009). The top 20 *in silico* structural matches for all three XLGs corresponded to heterotrimeric G protein Gα subunits, including GPA1 (Supplemental Table S1), with 99.9% to 100% confidence, and the conserved secondary structure patterning of the XLGs and GPA1 is evident when the Phyre<sup>2</sup> data are superimposed over an alignment of their Gα regions (Supplemental Fig. S1). As an independent secondary confirmation, the genTHREADER software was used to conduct additional fold recognition analyses (Jones, 1999a). genTHREADER returned 13 hits for each of the three XLGs that were classed as either certain ( $P < 0.0001$ ) or high ( $P = 0.0001-0.001$ ), all of which corresponded to the same 13 heterotrimeric G protein Gα structures, including that of GPA1 (Supplemental Table S2). In contrast to the high-confidence matching of the C-terminal domains of the XLGs with canonical Gα subunit structures, there were no high-ranking hits that matched the N-terminal domains of the XLGs.

We next examined the Gα region of XLG3 in greater detail by utilizing the I-TASSER server for protein structure modeling, assigning the empirically resolved crystal structure of GPA1 (Protein Data Bank no. 2XTZ:A; Jones et al., 2011a) as a template. For reference, the XLG3 Gα region encompasses residues 429 to 849, with residue 429 aligning to GPA1 residue 37 (Supplemental Fig. S1). To allow direct correlation, the exogenous MSGI tetrapeptide found at the N terminus of the GPA1 2XTZ crystal structure (Jones, 1999a) was computationally affixed to the XLG3 Gα domain; therefore, the first XLG3 native residue corresponds to residue 5 in the XLG3alpha.pdb structure (Supplemental File S1). The predicted XLG3 structure aligned closely to the crystal structure of GPA1

(Fig. 4; Supplemental Fig. S2). The theoretical model of the XLG3 Gα domain was validated as a reasonable approximation of the as yet undescribed XLG3 crystal structure, with a passing self-compatibility score (82.55% of residue 3D-1D [three dimension-one dimension] scores  $\geq 0.2$ ) from Verify-3D (Eisenberg et al., 1997), a ProSA Z-score of  $-7.2$  (Supplemental Fig. S3; Wiederstein and Sippl, 2007), and a plausible overall quality score of 83.894 (Supplemental Fig. S4) from ERRAT (Colovos and Yeates, 1993), which is designed to verify protein structures empirically determined from crystallography data. Together, the Phyre<sup>2</sup> and genTHREADER identification of structural homology to metazoan and plant Gα subunits, and the close alignment of the XLG3 and GPA1 Gα regions by I-TASSER, support XLG function as a component of the plant heterotrimeric G protein.

### XLG-Gβγ Interaction in Planta

To further test the hypothesis that XLGs function as Gα subunits, we utilized our recently developed multicassette pDOE vector BiFC system (Gookin and Assmann, 2014) with reduced nonspecific signal from self-assembly (Ohashi et al., 2012; Gookin and Assmann, 2014) to evaluate the XLG-Gβγ interactions in planta

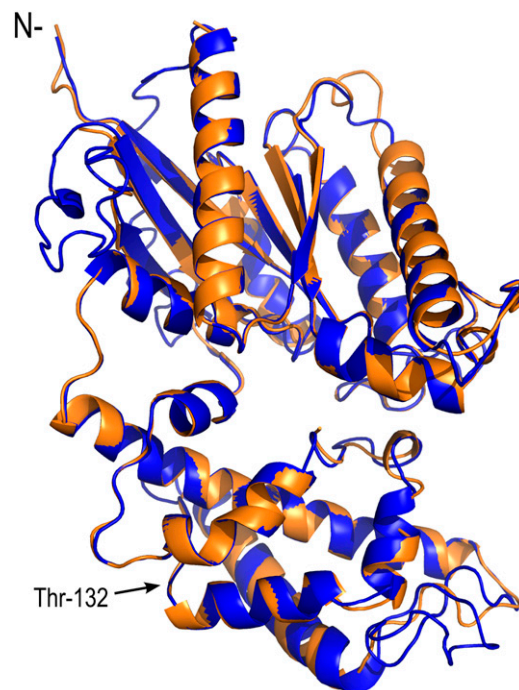
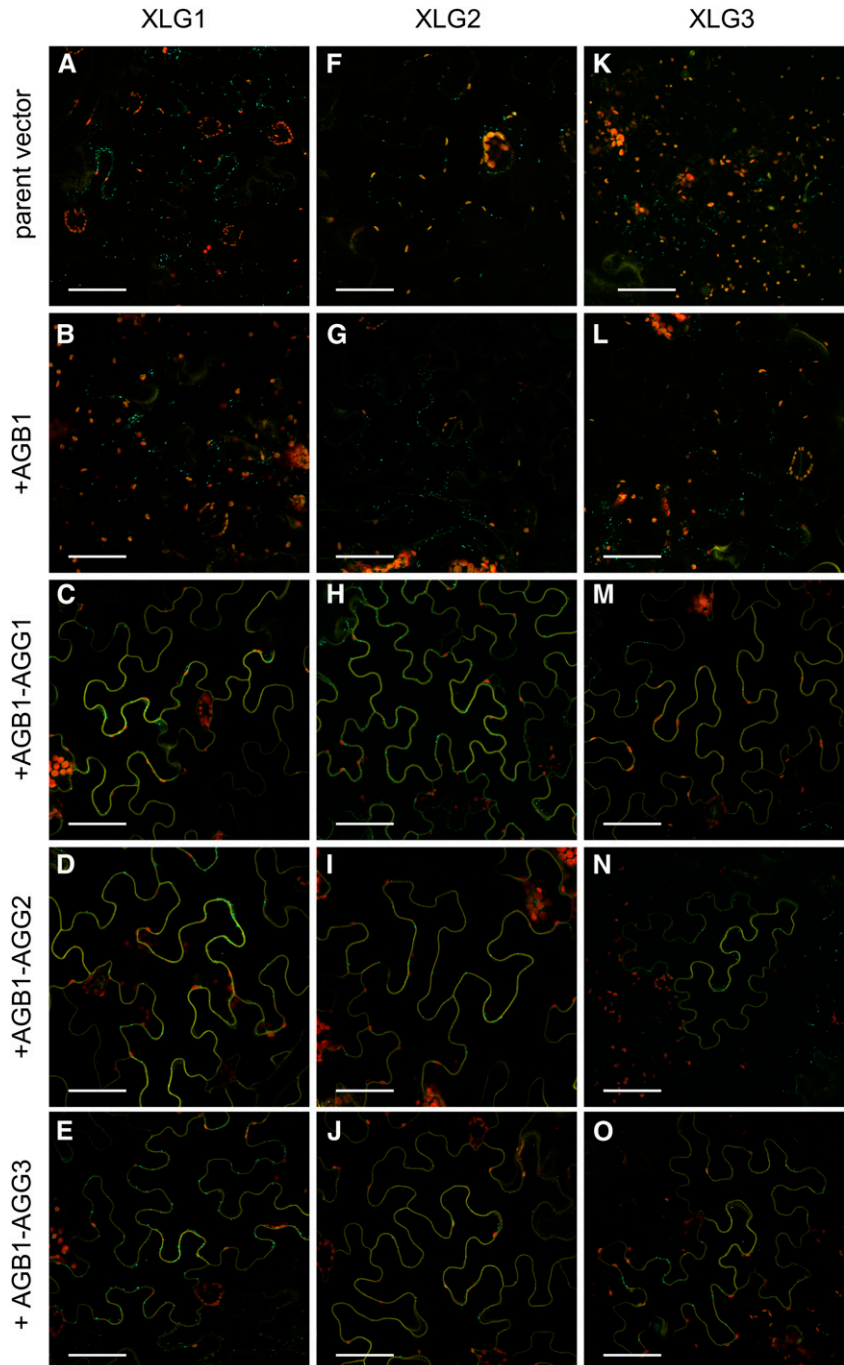


**Figure 4.** The XLG3 Gα-like region aligns closely to the crystal structure of GPA1. Superimposition of computationally derived XLG3 structural features on the empirically derived GPA1 crystal structure demonstrates their shared three-dimensional characteristics. Blue indicates the XLG3 Gα-like region, orange indicates the GPA1 Gα-like region, and N- indicates the N terminus of the Gα regions. Thr-132 marks the N<sub>ven</sub>210 insertion site in the αB-αC loop of GPA1 used for BiFC (Gookin and Assmann, 2014); each of the XLGs was modified at the analogous residue.

and assess subcellular localization. GPA1 interacts with AGB1-AGG dimers (Gookin and Assmann, 2014) when tagged internally, in a configuration consistent with a mammalian heterotrimer crystal structure (McCudden et al., 2005). Given the results of our yeast three-hybrid competition assay, we hypothesized that the XLGs and GPA1 would interact similarly with AGB1-AGG dimers. Accordingly, we inserted the NmVenus210 fragment into the middle of each XLG protein at a position analogous to the  $\alpha$ B- $\alpha$ C loop of GPA1 (Fig. 4) to generate XLG1L, XLG2L, and XLG3L parent vectors, to

which AGB1 was added to create three XLGL-CVen210:AGB1 test vectors. Negative control assays with the XLGL parent vectors (with an unfused CVen210 fragment in the second cassette) did not show any nonspecific BiFC signal (Fig. 5, A, F, and K). The XLGL-CVen210:AGB1 test constructs also showed zero to near zero signal (Fig. 5, B, G, and L). In all cases, positive transformation was confirmed by a vector-integrated XT-Golgi-mTq2 marker. Positive interaction between each XLGL fusion and AGB1 was only obtained when exogenous untagged AGG1 (Fig. 5, C, H, and M), AGG2 (Fig. 5, D, I, and N), or

**Figure 5.** XLG1, XLG2, and XLG3 interact with AGB1 at the plasma membrane in an AGG-dependent manner. In all assays, positive transformation is confirmed by Golgi-localized mTurquoise2 (mTq2) fluorescence from the pDOE XT-Golgi-mTq2 marker. A, The XLG1L-CVen210 parent vector does not produce nonspecific BiFC signal. B, The XLG1L-CVen210:AGB1 construct shows zero to near-zero signal in the absence of a coexpressed G $\gamma$  subunit. C, The XLG1L-CVen210:AGB1 construct produces BiFC signal in the presence of coexpressed AGG1. D, The XLG1L-CVen210:AGB1 construct produces BiFC signal in the presence of coexpressed AGG2. E, The XLG1L-CVen210:AGB1 construct produces BiFC signal in the presence of coexpressed AGG3. F, The XLG2L-CVen210 parent vector does not produce nonspecific BiFC signal. G, The XLG2L-CVen210:AGB1 construct shows zero to near-zero signal in the absence of a coexpressed G $\gamma$  subunit. H, The XLG2L-CVen210:AGB1 construct produces BiFC signal in the presence of coexpressed AGG1. I, The XLG2L-CVen210:AGB1 construct produces BiFC signal in the presence of coexpressed AGG2. J, The XLG2L-CVen210:AGB1 construct produces BiFC signal in the presence of coexpressed AGG3. K, The XLG3L-CVen210 parent vector does not produce nonspecific BiFC signal. L, The XLG3L-CVen210:AGB1 construct shows zero to near-zero signal in the absence of a coexpressed G $\gamma$  subunit. M, The XLG3L-CVen210:AGB1 construct produces BiFC signal in the presence of coexpressed AGG1. N, The XLG3L-CVen210:AGB1 construct produces BiFC signal in the presence of coexpressed AGG2. O, The XLG3L-CVen210:AGB1 construct produces BiFC signal in the presence of coexpressed AGG3. Vectors were agroinfiltrated into *N. benthamiana* leaves at an optical density at 600 nm (OD<sub>600</sub>) of 0.0075 to 0.01, and images were acquired 57 to 60 h post infiltration. Yellow indicates mVenus BiFC, blue indicates mTq2, and red indicates chlorophyll autofluorescence. Bars = 50  $\mu$ m.



AGG3 (Fig. 5, E, J, and O) subunits were provided via cotransformation with a second vector. Population level images show the reproducibility of these assays (Supplemental Fig. S5).

To identify the subcellular localization of the XLG-AGB1-AGG heterotrimers, we performed high-magnification (63× and 95×) colocalization experiments with the plasma membrane staining dye FM4-64 (Bolte et al., 2004) and found that the interaction occurs specifically at the plasma membrane (Fig. 6). Furthermore, the XLG-Gβγ heterotrimers do not colocalize with internalizing FM4-64-labeled vesicles (Fig. 6, J, K, and L). These results complement our yeast data and show a dependency on all three subunits for a positive XLG-AGB1 interaction at the plasma membrane in planta.

### XLG Subcellular Localization

All three *Arabidopsis* XLG proteins were originally described as nuclear resident proteins (Ding et al.,

2008), but Maruta et al. (2015) showed XLG1 localization at the plasma membrane and XLG2 and XLG3 localization at both the plasma membrane and nucleus.

To reassess XLG subcellular localization patterns, we created UBIQUITIN10 promoter-driven XLG:mVenus fusions. We reasoned that the use of the optimized and bright monomeric mVenus fluoroprotein, in combination with the slower kinetics of the UBIQUITIN10 promoter-driven expression, would allow for enhanced temporal resolution (Gookin and Assmann, 2014). Analysis of XLG:mVenus fusions transiently expressed in *Nicotiana benthamiana* leaves showed that XLG1 is primarily extranuclear, with nuclear signal ranging from not detectable to weak (Fig. 7, A and B). XLG2:mVenus localization varied from predominantly nuclear (Fig. 7C) to an even distribution between nucleus and the cytoplasm (Fig. 7D). XLG3:mVenus consistently localized to both the nucleus and cytoplasm (Fig. 7, E and F) in every agroinfiltration experiment. The nuclear accumulation patterns of the three XLGs were

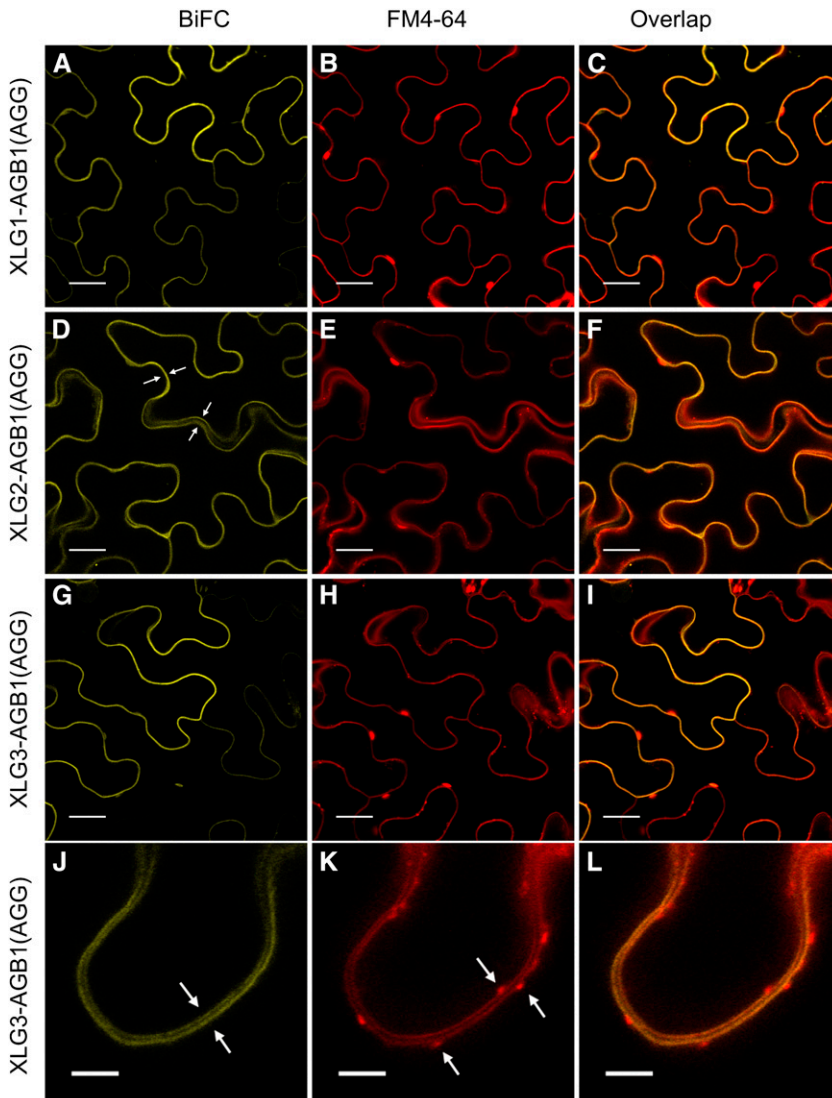
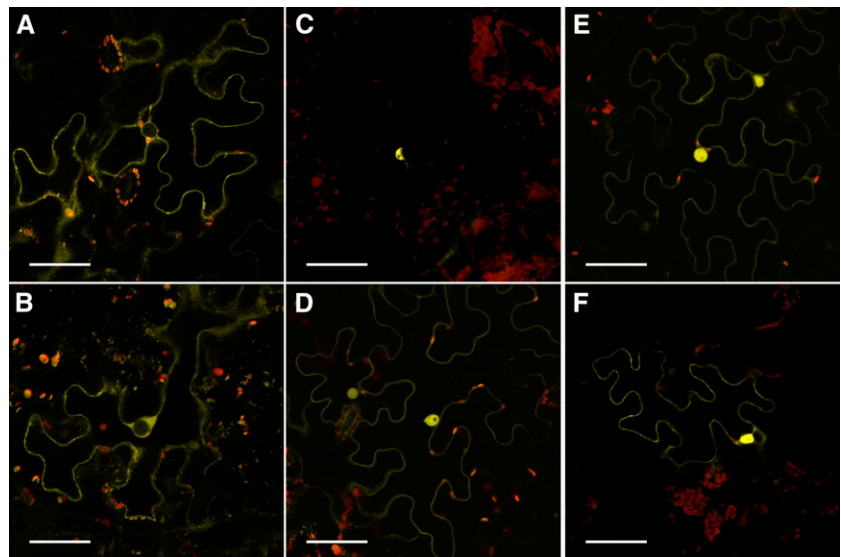


**Figure 6.** XLG-based heterotrimers localize specifically to FM4-64-marked plasma membranes. The UBIQUITIN10 promoter-driven XLG-AGB1 test constructs were cotransformed with the 35S-driven pDOE- $\gamma_1\gamma_2$  vector (Gookin and Assmann, 2014) as a source of untagged AGG1 and AGG2. A, XLG1 interacts with AGB1. B, FM4-64 stains the plasma membrane. C, XLG1-AGB1 BiFC signal overlaps with the FM4-64-marked plasma membrane. D, XLG2 interacts with AGB1. The four white arrows mark the plasma membranes of two adjacent transformed cells traversing in and out of the 1.1- $\mu\text{m}$  focal plane. E, FM4-64 marks the plasma membrane. F, XLG2-AGB1 BiFC signal overlaps with the FM4-64-marked plasma membrane. G, XLG3 interacts with AGB1. H, FM4-64 stains the plasma membrane. I, XLG3-AGB1 BiFC signal overlaps with the FM4-64-marked plasma membrane. J, High-resolution/magnification image of the XLG3-AGB1 BiFC signal visible at the two distinct plasma membranes of two adjacent cells, marked with white arrows. K, FM4-64 specifically labels the two distinct plasma membranes. White arrows mark FM4-64-labeled vesicles. L, XLG3-AGB1 BiFC signal overlaps with the two distinct FM4-64-marked plasma membranes but not with the FM4-64-marked vesicles. Test vectors were agroinfiltrated into *N. benthamiana* leaves at an  $\text{OD}_{600}$  of 0.0075, and images were acquired 62 to 67 h post infiltration. FM4-64 was infiltrated at 50  $\mu\text{M}$  just prior to imaging. Images in A to I were acquired at 63× magnification with a 1.1- $\mu\text{m}$  optical slice; bars = 20  $\mu\text{m}$ . Images in J to L were acquired at 95× (63× magnification plus a 1.5× zoom of the scan area during image acquisition; 0.09  $\mu\text{m}$  per pixel resolution); bars = 5  $\mu\text{m}$ . Yellow indicates mVenus BiFC, and red indicates FM4-64.

**Figure 7.** Subcellular localization of Arabidopsis XLG proteins in *N. benthamiana* leaves. A to D, UBIQUITIN10 promoter-driven XLG:mVenus fusions show differing localization patterns. A and B, XLG1 is predominantly extranuclear with nearly undetectable (A) to very weak (B) nuclear signal. C and D, XLG2 varies between strong nuclear signal (C) and signal evenly divided between the nucleus and cytoplasm (D). E and F, XLG3 consistently localizes to the nucleus and the cytoplasm. Agro-infiltrations of *N. benthamiana* leaves were performed at an OD<sub>600</sub> of 0.0075 to 0.01 and imaged at 60 to 68 h, except for F, which was imaged at 6 d post infiltration. Yellow indicates mVenus, blue indicates mTq2, and red indicates chlorophyll autofluorescence. Bars = 50  $\mu$ m.



confirmed in high-magnification (63 $\times$ ) colocalization experiments, with mTq2-tagged nuclear specific histone 2B (Heidstra et al., 2004) colocalizing with the XLGs in the nucleus (Supplemental Fig. S6). In comparison, our BiFC results show that all three XLGs interact with all three G $\beta$  $\gamma$  dimers at the cell periphery (Fig. 5; Supplemental Fig. S5), suggesting that coexpression of partner subunits is a key determinant of XLG intracellular location.

Sequence analysis of the three XLGs using the PredictProtein software suite (Yachdav et al., 2014) only identified the classic monopartite nuclear localization signal (NLS) present in XLG3 (RRKKKKK), previously identified by Ding et al. (2008). We next used computational regular expression to search the set of NLSs identified and functionally characterized in cv BY-2 tobacco (*Nicotiana tabacum*) cells by Kosugi et al. (2009). Our search identified a potential noncanonical NLS in XLG2 (KKRAKiaCAVF) through a partial match with CAVF (Fig. 8A). This potential XLG2 NLS resides within a small stretch of sequence that is semi-conserved among the XLGs (Fig. 8B). Accordingly, we assessed the NLS functionality of this region. We used residue substitution to modify the XLG1 sequence to mirror XLG2 in this stretch (Fig. 8B, arrows) and expressed the resultant XLG1m1:mVenus fusion in *N. benthamiana* leaves. In contrast to XLG1 (Fig. 7, A and B; Supplemental Fig. S6A), XLG1m1 produced strong nuclear signal (Fig. 8C), specifically colocalizing with the nucleus-specific signal of mTq2:histone 2B (Fig. 8, D and F) and providing evidence that the atypical NLS of XLG2 is functional.

Since XLG2 and XLG3 also show both nuclear and extranuclear localization, we analyzed these sequences in search of a nuclear export signal (NES). We did not find a direct match to the classic consensus pattern for a Leu-rich NES (Xu et al., 2012); therefore, we used computational regular expression to search the set of validated NESs identified by Kosugi et al. (2008). Our

analyses based on hydrophobic residue spacing identified a potential unconventional class 2 NES in XLG3 (LELRILKL; Fig. 9A). Two of these residues (I and the final L) were also weakly identified by NetNES (la Cour et al., 2004), suggesting the presence of a NES. We created two residue substitution mutants to map the domain, in which conserved hydrophobic residues that are functionally important to the motif were substituted with Gly (lowercase g): XLG3m1:mVenus (gEgRILKL) and XLG3m2:mVenus (LELRggKg; Fig. 9A). Both XLG3m1 and XLG3m2 produced strong nuclear signal (Fig. 9, B–D), demonstrating that the identified NES regulates XLG3 subcellular localization.

We next investigated XLG3:mVenus localization upon the coexpression of 35S-driven untagged AGB1-AGG1 and AGB1-AGG2 dimers. In both assays, XLG3 was sequestered at the plasma membrane, and in many cases, the nucleus was devoid of fluorescent signal (Fig. 10). These results provide evidence that XLG3 localization is dynamic and, in conjunction with our BiFC results, demonstrate that the plasma membrane is the site of XLG-G $\beta$  $\gamma$  interaction.

#### *xlg* Mutants Recapitulate *agb1/agg1* and *agb1/agg2* Phenotypes

The majority of G protein-related phenotypes have been characterized for *gpa1* and *agb1* mutants; however, for a growing but not yet comprehensive number of phenotypes, details have been described for G $\gamma$  subunit mutants as well. Comparison of published phenotypes suggests that while AGB1 (the only G $\beta$  subunit) participates in all G protein-mediated processes, the majority of *gpa1* phenotypes are restricted to recapitulation in *agg3* mutants. For example, hypersensitivity to abscisic acid during germination (Ullah et al., 2002; Chakravorty et al., 2011), decreased etiolated hypocotyl elongation (Ullah et al., 2001; Chakravorty et al., 2011),

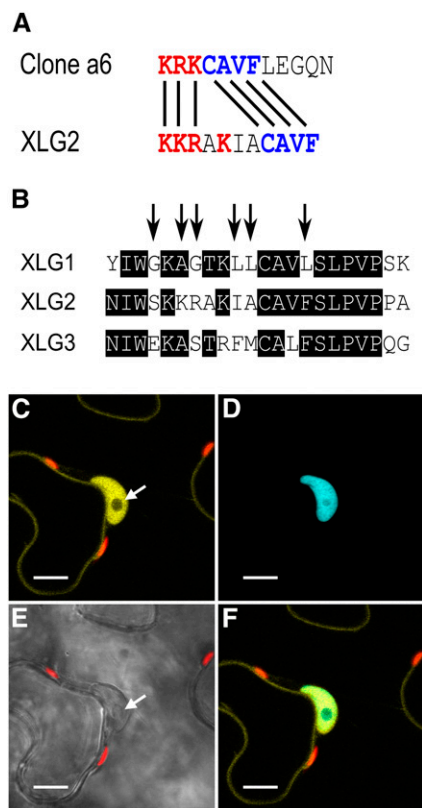


**Figure 8.** XLG2 has a functional NLS. A, The XLG2 NLS has a similar basic-positive patch of residues (red) and a CAVF motif (blue) identical to the empirically validated clone a6 sequence (Kosugi et al., 2009). B, The XLG2 NLS resides in a semiconserved stretch of sequence in the XLG family starting at XLG2 residue 424, and the arrows show the XLG1 residues mutated to mirror XLG2 to create the XLG1m1 construct. XLG1m1:mVenus fusions localized to the nucleus in *N. benthamiana* leaves, demonstrating that the XLG2 NLS is a functional regulatory domain. (Compare with XLG1:mVenus localization in Figure 7, A and B.) C to F, Agroinfiltration of XLG1m1:mVenus into *N. benthamiana* leaves at an OD<sub>600</sub> of 0.0075 to 0.01 and imaged 48 h later at 63× magnification. C, XLG1m1:mVenus localizes to the interior of the nucleus and at the plasma membrane; the nucleolus (white arrow) does not appreciably accrue XLG1m1. D, The nucleus is specifically marked by mTq2:histone 2B. E, The nucleus and nucleolus (white arrow) are clearly visible in the bright-field channel. F, XLG1m1:mVenus and mTq2:histone 2B colocalization is specific to the nucleus. Yellow indicates mVenus, blue indicates mTq2, and red indicates chlorophyll autofluorescence. Bars = 10 μm.

round leaf morphology (Ullah et al., 2001; Chakravorty et al., 2011), hyposensitivity to abscisic acid inhibition of stomatal opening (Wang et al., 2001; Chakravorty et al., 2011), shortened silique morphology (Trusov et al., 2008; Chakravorty et al., 2011), and round seed (Chakravorty et al., 2011) phenotypes are all similar in *gpa1* and *agg3* mutants. The recapitulation of *gpa1* phenotypes in *agg3* mutants correlates well with the GPA1-AGB1/AGG3 binding specificity demonstrated in Figure 1. Conversely, a number of *agg1* and *agg2* phenotypes are recapitulated in *agb1*, but opposite or wild-type phenotypes are observed in *gpa1* mutants

(Table I). Our yeast three-hybrid results, showing that AGB1/AGG1 and AGB1/AGG2 interact preferentially with XLGs over GPA1, raise the intriguing possibility that XLGs form signaling complexes with Gβγ and may especially be involved in *agb1/agg1* and *agb1/agg2* phenotypes. We selected several phenotypes present in *agb1* mutants, but absent from (or not yet assessed in) *gpa1* mutants, for examination in *xlg* mutants. The four phenotypes we selected were NaCl, tunicamycin, and D-Glc hypersensitivity and increased stomatal density.

Colaneri et al. (2014) showed that Arabidopsis *agb1* mutants are hypersensitive to NaCl, while *gpa1* is hyposensitive to NaCl. Urano et al. (2014) examined Gα mutants available in rice and maize (*Zea mays*) and found that the Gα mutants were, much like *gpa1* mutants in Arabidopsis, hyposensitive to salt treatment. The hypersensitivity of Gβ mutants to NaCl, and the hyposensitivity of Gα mutants, suggested that NaCl

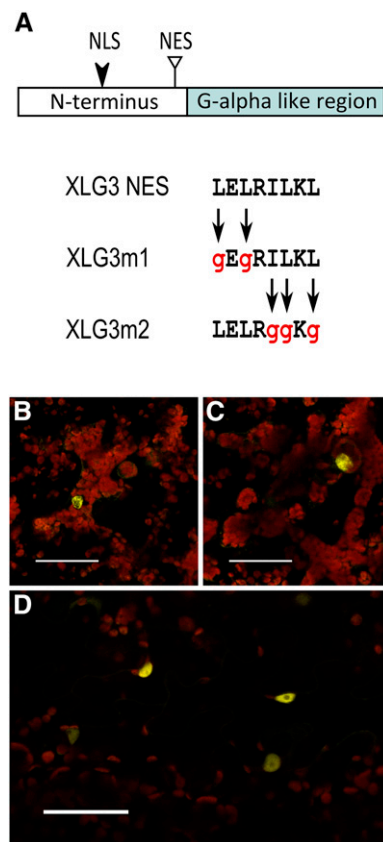


**Figure 9.** XLG3 has a functional NES. A, The N-terminal domain of XLG3 has an unconventional NES (triangle) located just upstream of the Gα-like region. The XLG3 NES was mutated by substituting hydrophobic residues at the N terminus (XLG3m1) or the C terminus (XLG3m2) of the domain with Gly residues. Both mutants showed nearly exclusive nuclear localization. B and C, XLG3m1 nuclear localization in two focal planes of the same mesophyll cells. D, XLG3m2 nuclear localization in epidermal pavement cells. Agroinfiltrations of *N. benthamiana* leaves were performed at an OD<sub>600</sub> of 0.0075 to 0.01 and imaged 50 to 55 h later. Yellow indicates mVenus, blue indicates mTq2, and red indicates chlorophyll autofluorescence. Bars = 50 μm.



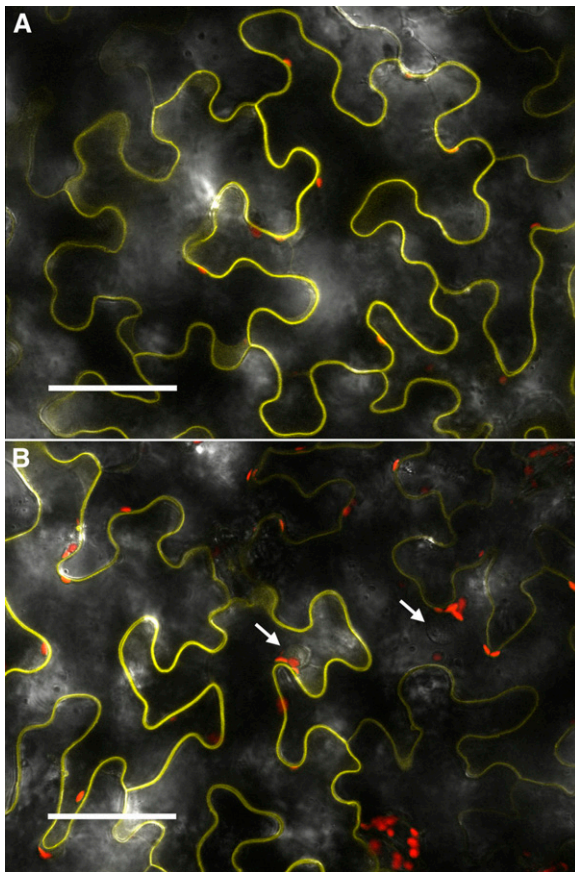


**Figure 10.** Overexpression of  $G\beta\gamma$  dimers sequesters XLG3 at the plasma membrane. XLG3::mVenus driven by the UBIQUITIN10 promoter is retained at the plasma membrane when coexpressed with 35S-driven AGB1-AGG1 (A) or AGB1-AGG2 (B) dimer. (Compare with localization of the XLG3::mVenus fusion protein in the absence of additional  $G\beta\gamma$  in Figure 7, E and F.) Note the lack of nuclear signal in two nuclei (white arrows) visible in the bright-field channel. The plasma membrane retention was consistent over time; these images were acquired 6 d post infiltration of *N. benthamiana* leaves at a final OD<sub>600</sub> of 0.0075 for XLG3 and 0.025 for  $G\beta\gamma$  dimers. Yellow indicates mVenus, blue indicates mTq2, and red indicates chlorophyll autofluorescence. Bars = 50  $\mu$ m.

sensitivity is a candidate for a potential *xlg* phenotype. Colaneri et al. (2014) found that *agg1* and *agg2* single mutants were not hypersensitive to NaCl; however, the *agg1-1c agg2-1 agg3-1* triple mutant appeared hypersensitive to NaCl.

As we hypothesize that *agg1*- and/or *agg2*-mediated phenotypes are a potential indicator of XLG involvement, we first clarified  $G\gamma$  subunit involvement in NaCl sensitivity by testing all single, double, and triple mutant combinations of  $G\gamma$  mutants and deduced that AGG1 and AGG2 play redundant roles in NaCl sensitivity: *agg1-1c agg2-1* double mutants displayed a similar NaCl hypersensitivity to the *agb1-2* mutant or the *agg* triple mutant (Fig. 11A). AGG3 is not involved in salt sensitivity, as all *agg3*-containing genotypes, aside from the *agg* triple mutant, displayed wild-type sensitivity (Fig. 11A). We next investigated the salinity

phenotype of the *xlg* single and triple mutants. An increased number of *xlg* single mutant seedlings, as compared with wild-type seedlings, displayed slight chlorosis, indicated by the arrows in Figure 11B, on 150 mM NaCl plates. The chlorosis was generally limited to one or two leaves in the single *xlg* mutants and was much more pronounced in both the *agb1-2* mutant and the *xlg* triple mutant (Fig. 11B). Similarly, when compared with the wild type, the *agb1-2* and *xlg* triple mutants each displayed a clear decrease in seedling survival (Fig. 11C). Therefore, the *agb1-2, agg1-1c agg2-1* double, and *xlg* triple mutants displayed similar NaCl hypersensitivity phenotypes, suggesting the possibility that up to six heterotrimer combinations, XLG1/AGB1/AGG1, XLG1/AGB1/AGG2, XLG2/AGB1/AGG1, XLG2/AGB1/AGG2, XLG3/AGB1/AGG1, and XLG3/AGB1/AGG2, function in salt sensitivity.

Another potential *xlg* phenotype is hypersensitivity to tunicamycin, a mixture of homologous compounds that block nitrogen-linked glycosylation, thereby inducing the unfolded protein response (UPR; Schröder and Kaufman, 2005), a stress response initiated in the endoplasmic reticulum when the cellular protein production and folding machinery is overcome, for example by inhibited posttranslational modification (Koizumi et al., 2001; Schröder and Kaufman, 2005). Wang et al. (2007) initially reported that the *agb1-2* mutant was hypersensitive to tunicamycin, while *gpa1-4* displayed wild-type sensitivity. Contrary to the initial report, Chen and Brandizzi (2012) reported that multiple *agb1* mutants, including *agb1-2*, were hypersensitive to tunicamycin in a plate-based seedling assay assessing recovery from tunicamycin. Similar to the report from Chen and Brandizzi (2012), in our hands, *agb1-2* was more sensitive than the wild type to tunicamycin, with 0.15  $\mu$ M tunicamycin the optimal concentration for differentiating *agb1-2* from the wild type.

We then investigated the  $G\gamma$  subunit mutants in the tunicamycin recovery assay. The *agg1-1c agg2-1* double mutant and *agg* triple mutant, like *agb1-2*, were particularly hypersensitive to tunicamycin. As with the salt assay, the *gpa1* and single  $G\gamma$  mutants were not hypersensitive to tunicamycin (Fig. 12A), suggesting that AGG1 and AGG2 play redundant roles and that tunicamycin sensitivity is a candidate *xlg* phenotype. As seen in Figure 12B, the *xlg* single mutants, particularly *xlg2-1* and *xlg3-1*, were indeed hypersensitive to tunicamycin, showing a clear increase in the number of stunted seedlings as compared with the wild type (Fig. 12, B and C). The *xlg* triple mutant fully recapitulated the *agb1-2* hypersensitivity phenotype, with approximately 90% of seedlings of both genotypes unable to recover from the treatment (Fig. 12B) and scored as dead (Fig. 12C). The similarity of tunicamycin hypersensitivity phenotypes suggests that the XLGs may function in a heterotrimer with AGB1/AGG1 and AGB1/AGG2.

A third potential *xlg* phenotype is the sensitivity of *agb1* to D-Glc in postgermination development. It has been demonstrated that *agb1-2* is hypersensitive to

**Table 1.** Summary of phenotypic differences between *gpa1* and *agb1* mutants, and participation of the XLGs in these phenotypes

G protein phenotypes from the literature in which *gpa1* and *agb1* mutants display opposite or different phenotypes are listed. Phenotypes of *gpa1*, *agb1*, *xlg*, *agg1/agg2*, and *agg3* mutants are annotated as hypersensitive, hyposensitive, or wild type for responses. Morphological phenotypes are annotated as increased, decreased, or wild type. New results from this article are included in boldface. Phenotypes were often found to be similar or aligned between *xlg*, *agb1*, and *agg1/agg2* mutants. References, in square brackets, are as follows: [1] Llorente et al. (2005); [2] Trusov et al. (2006); [3] Zhu et al. (2009); [4] Maruta et al. (2015); [5] Trusov et al. (2007); [6] Chakravorty et al. (2011); [7] Ding et al. (2008); [8] Chen et al. (2006); [9] Li et al. (2012); [10] Ullah et al. (2003); [11] Pandey et al. (2008); [12] Colaneri et al. (2014); [13] Chen and Brandizzi (2012); [14] Wang et al. (2006); [15] Zhang et al. (2008); and [16] Nilson and Assmann (2010).

Phenotype	Genotypes				
	<i>gpa1</i>	<i>agb1</i>	<i>xlgs</i>	<i>agg1/2</i>	<i>agg3</i>
Susceptibility to pathogens	↓ Decreased [1,2]	↑ Increased [1,2,3,4]	↑ Increased [3,4]	↑ Increased [5]	– Wild type [6]
Primary root growth rate/length	– Wild type [7,8]	↑ Increased [7,8]	↑ Increased [7]		– Wild type [9]
Lateral root proliferation	↓ Decreased [10]	↑ Increased [10]	↑ Increased [7]	↑ Increased [5]	– Wild type [6]
Root waving and skewing	↓ Wild type/minor decrease [11]	↓ Decreased [11]	↓ Decreased [11]		
Sensitivity to salt post germination	↓ Hyposensitive [12]	↑ Hypersensitive [12]	↑ <b>Hypersensitive</b>	↑ <b>Hypersensitive</b>	– <b>Wild type</b>
Sensitivity to tunicamycin post germination	– <b>Wild type</b>	↑ Hypersensitive <sup>a</sup> [13]	↑ <b>Hypersensitive</b>	↑ <b>Hypersensitive</b>	– <b>Wild type</b>
Sensitivity to D-Glc post germination	– <b>Wild type</b>	↑ Hypersensitive [14]	↑ <b>Hypersensitive</b>	↑ <b>Hypersensitive</b>	– <b>Wild type</b>
Stomatal density/index	↓ Decreased [15,16]	↑ Increased [15]	↑ <b>Increased</b>	↑ <b>Increased</b>	– Wild type [6]

<sup>a</sup>Wang et al. (2007) described the opposite, with *agb1* hyposensitive.

D-Glc when grown on plates (Wang et al., 2006). Additionally, the ARABIDOPSIS REGULATOR OF G PROTEIN SIGNALING protein (AtRGS1) has been implicated in D-Glc signaling, as *rgs1* seedlings are hyposensitive to D-Glc (Chen and Jones, 2004), and AtRGS1 internalizes upon D-Glc treatment in an AGB1- and AGG1-/AGG2-dependent manner (Urano et al., 2012b). We germinated seeds of the G protein mutants on medium supplemented with 1% or 6% (w/v) D-Glc under high-light conditions to synchronize germination (Trusov et al., 2007) and then allowed seedlings to grow under low-light conditions, to replicate the assay conducted by Wang et al. (2006). However, in our hands, even 6% (w/v) D-Glc was not sufficient to severely repress the development of *agb1-2* seedlings. Instead, the increased stress placed upon the *agb1-2* seedlings was manifested in increased anthocyanin production at higher D-Glc concentrations; therefore, we quantitatively assessed the D-Glc stress phenotype by measuring anthocyanin content (Mancinelli et al., 1991).

The anthocyanin content of all genotypes was similarly negligible when grown on medium supplemented with 1% (w/v) D-Glc (Fig. 13). However, anthocyanin content in 6% (w/v) D-Glc was elevated in *agb1-2* and all *agg1-1c*-containing genotypes (*agg1-1c*, *agg1-1c agg2-1*, *agg1-1c agg3-1*, and the *agg* triple mutant) but not in *gpa1-4* (Fig. 13A). Therefore, D-Glc sensitivity fits the criteria of an *agb1/agg1* or *agb1/agg2* phenotype that lacks GPA1 involvement. When we repeated the assay with *xlg* mutants, the *xlg* triple mutant reproduced the *agb1-2* phenotype (Fig. 13B). These results suggest that XLG/AGB1/AGG1 heterotrimers function in postgermination D-Glc sensitivity.

Finally, we investigated the stomatal density phenotype of the G protein mutants. Zhang et al. (2008) found that *gpa1* and *agb1* mutants displayed a lower and higher stomatal density than the wild type,

respectively, in cotyledons. Chakravorty et al. (2011) showed that the *agg3* mutants resembled the wild type in cotyledon stomatal density. These results suggested that stomatal density is another candidate phenotype for XLG involvement.

The cotyledons of *gpa1* and *agb1* mutants displayed lower and higher stomatal density than the wild type (Fig. 14, A, C, D, and E), respectively, in agreement with the results of Zhang et al. (2008). As seen in Figure 14A, the *agg1-1c* mutant also displayed an increase in stomatal density, as did the *agg1-1c agg2-1* double mutant and the *agg* triple mutant. Of the Gγ mutants, the *agg1-1c agg2-1* double mutant displayed the largest increase in stomatal density, higher even than *agb1* or the *agg* triple mutant. All *agg3*-containing genotypes displayed a slight, but not statistically significant, decrease in stomatal density as compared with the wild type. Like the *agb1* mutant, the *xlg* triple mutant displayed an increase in stomatal density (Fig. 14, B, C, E, and F), indicating that XLG/AGB1/AGG1,2 heterotrimers repress stomatal development. In fact, the stomatal density of the *xlg* triple mutant was greater than that of the *agb1* mutant ( $P = 0.02$ , Student's *t* test). These results may indicate a dual function for AGB1, with GPA1/AGB1/AGG3 heterotrimers stimulating stomatal development and XLG/AGB1/AGG1 and XLG/AGB1/AGG2 heterotrimers repressing stomatal development. This would explain the greater severity of the *agg1-1c agg2-1* (Fig. 14A) and *xlg* triple (Fig. 14B) mutants when compared with *agb1* and the *agg* triple mutant.

## DISCUSSION

### XLGs as Noncanonical Gα Proteins

Here, we make a case that the three XLGs are non-canonical Gα subunits that function within the

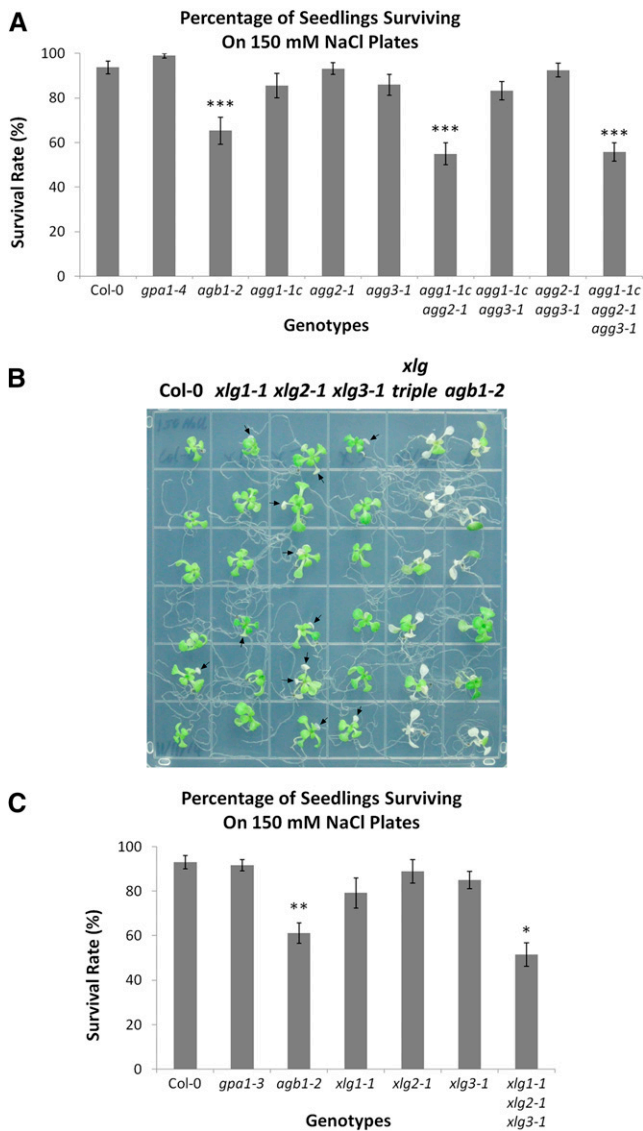


**Figure 11.** *agb1*, *agg1* *agg2*, and the *xlg* triple mutant are hypersensitive to salt. Seeds were sown and germinated on 0.5× Murashige and Skoog (MS) plates (1% [w/v] Suc and 1% [w/v] agar). After 9 d of growth, seedlings were transferred to 0.5× MS plates (1% [w/v] Suc and 1% [w/v] agar) supplemented with 150 mM NaCl. Seedling survival was scored once seedling death was apparent in the most severely affected genotypes (14–21 d). Assays were conducted with mutants of the G $\gamma$  subunits (A) and *xlg* mutants (B and C). A representative image of the results with the *xlg* mutants and *agb1-2* is shown in B, and quantification is shown in C. Columbia-0 (Col-0), *agb1*, and *gpa1* controls were included in both assays. In B, *xlg triple* refers to the *xlg1-1 xlg2-1 xlg3-1* mutant. Significant differences from Col-0 (Student’s *t* test) are indicated: \*, *P* < 0.05 to 0.01; \*\*, *P* < 0.01 to 0.001; and \*\*\*, *P* < 0.001. All values are means  $\pm$  SE.

heterotrimeric G protein complex. The sole canonical G $\alpha$  protein subunit in Arabidopsis is GPA1, originally identified by Ma et al. (1990). In 1999, we reported the identification of the first noncanonical G $\alpha$ -like protein in plants, Arabidopsis XLG1, and we demonstrated that the XLG1 protein binds GTP (Lee and Assmann, 1999). Analysis by Maruta et al. (2015) suggests that

XLGs evolved from canonical G $\alpha$  subunits. Furthermore, our in silico structural analysis shows that the XLG3 G $\alpha$  domain and GPA1 are strikingly similar (Fig. 4; Supplemental Figs. S1 and S2), suggesting that GPA1 and XLG3 may share a common binding surface on

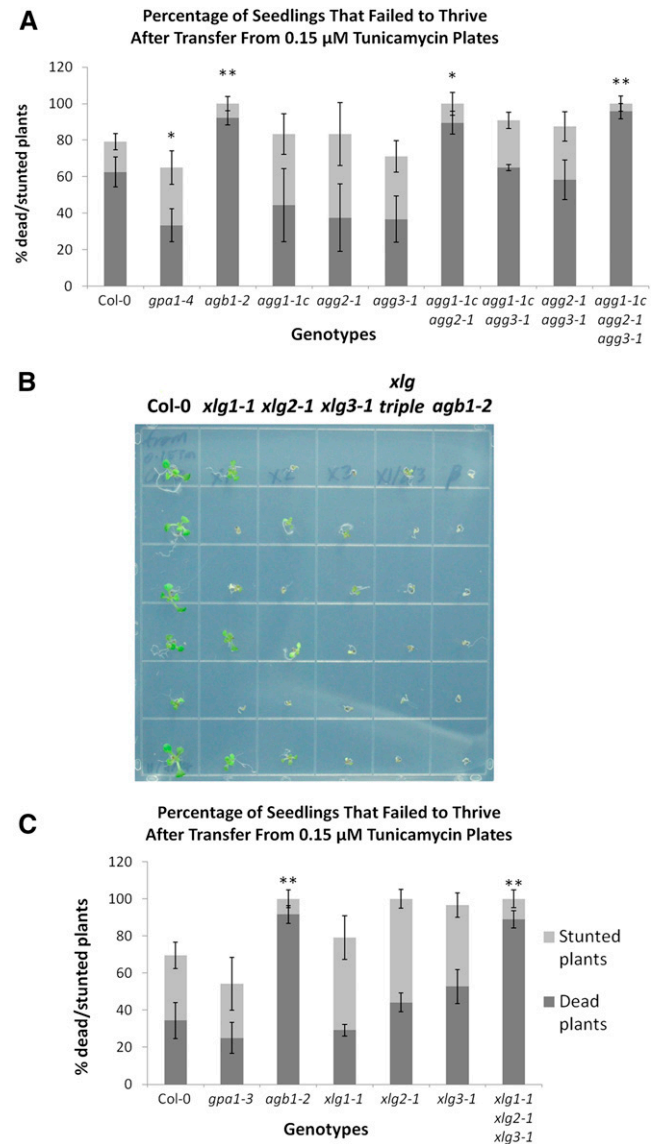


**Figure 12.** *agb1*, *agg1* *agg2*, and the *xlg* triple mutant are hypersensitive to tunicamycin. Seeds were sown and germinated on 0.5× MS plates (1% [w/v] Suc and 1% [w/v] agar) supplemented with 0.15  $\mu$ M tunicamycin. After 6 d of growth, seedlings were transferred to 0.5× MS plates (1% [w/v] Suc and 1% [w/v] agar) and allowed to recover for an additional 10 d before being scored, as outlined in “Materials and Methods.” Seedlings that failed to thrive (stunted + dead seedlings) are presented for mutants of the G $\gamma$  subunits (A) and *xlg* mutants (B and C). A representative image of the results with the *xlg* mutants and *agb1-2* is shown in B, and quantification is shown in C. Col-0, *agb1*, and *gpa1* controls were included in both assays. In B, *xlg triple* refers to the *xlg1-1 xlg2-1 xlg3-1* mutant. Significant differences from Col-0 (Student’s *t* test) are indicated: \*, *P* < 0.05 to 0.01; and \*\*, *P* < 0.01 to 0.001. All values are means  $\pm$  SE.

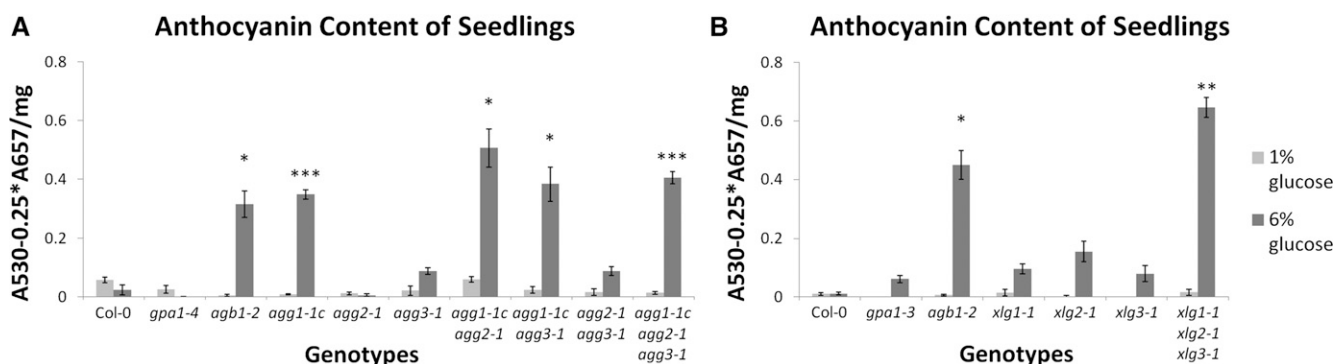


**Figure 13.** *agb1*, *agg1*, and the *xlg* triple mutant are hypersensitive to D-Glc. Seeds were sown on 0.5× MS plates (1% [w/v] agar) supplemented with 1% or 6% (w/v) D-Glc. Seeds were germinated under 120  $\mu\text{mol m}^{-2} \text{s}^{-1}$  white light for 1 d, then light intensity was dimmed to 60  $\mu\text{mol m}^{-2} \text{s}^{-1}$ . After 24 d of growth in long-day conditions, anthocyanins were extracted and quantified for mutants of the  $G\gamma$  subunits (A) and *xlg* mutants (B). Col-0, *agb1*, and *gpa1* controls were included in both assays. Significant differences from Col-0 (Student's *t* test) are indicated: \*,  $P < 0.05$  to 0.01; \*\*,  $P < 0.01$  to 0.001; and \*\*\*,  $P < 0.001$ . All values are means  $\pm$  se.

$G\beta\gamma$ . The intermolecular arrangement of canonical  $G\alpha$  with  $G\beta\gamma$  in the heterotrimer is well established (Wall et al., 1998), and all three XLG family members show strong structural conservation of their  $G\alpha$  region with the empirically derived GPA1 structure (Supplemental Tables S1 and S2). In our yeast three-hybrid assays, we observed that GPA1 and XLG3 are capable of competing with each other for binding of the AGB1/AGG3 dimer (Fig. 3). Competition between GPA1 and XLG3 for  $G\beta\gamma$ -binding also suggests that GPA1 and XLG3 share a common binding surface on  $G\beta\gamma$ , supporting the hypothesis that XLGs and GPA1 bind  $G\beta\gamma$  in a similar conformation. This idea is further supported by the efficient interaction between XLGs and  $G\beta\gamma$  dimers that is observed (Fig. 5) upon insertion of the NmVenus210 fragment into a position analogous to the  $\alpha\text{B-}\alpha\text{C}$  loop insertion, a position that also enables the observation of GPA1 interaction with AGB1-AGG dimers in BiFC (Gookin and Assmann, 2014). Our protein-protein interaction data and phenotypic analyses, in combination with the genetic evidence provided by Maruta et al. (2015), suggest that the recapitulation of *agb1* phenotypes that we observe in the *xlg* triple mutant is likely due to the XLGs, AGB1, and AGG1/AGG2 functioning in the same pathways. In short, we provide evidence from several different approaches that all three XLG proteins participate within a heterotrimeric G protein complex.

One impediment to denoting XLGs as true  $G\alpha$  subunits relates to the fact that bona fide  $G\alpha$  subunits display a GTP/GDP switch during the activation/inactivation cycle, and while XLGs are GTP-/GDP-binding and GTPase-capable proteins (Heo et al., 2012), this switch has not been shown to control activation/inactivation. However, in truth, the single canonical Arabidopsis  $G\alpha$  subunit, GPA1, also falls short of fulfilling this stringent criterion. The activation/inactivation dynamics of GPA1 are poorly understood, due to unusual GTP-binding and hydrolysis kinetics (Johnston et al., 2007, 2008; Urano et al., 2012a), regulation by the atypical seven transmembrane domain containing

AtRGS1 (Chen et al., 2003; Jones et al., 2011b; Urano et al., 2012b), and functional interactions between receptor-like kinases and G proteins (Bommert et al., 2013; Liu et al., 2013; Ishida et al., 2014). Indeed, the in planta GTP-/GDP-binding kinetics of GPA1, as well as those of the XLGs, are unknown. Because  $G\beta\gamma$  availability may alter the ratio of GTP-bound versus GDP-bound  $G\alpha$  subunits, the addition of XLGs as potentially competing  $G\beta\gamma$  interactors may have implications for the in planta activity of the  $G\alpha$  pool, including GPA1.

It should be noted that we provide direct evidence for GPA1 and XLG3 competition for  $G\beta\gamma$  binding only in yeast; it would be valuable to perform analogous experiments in planta as well. Such experiments may be technically challenging, given previously noted difficulties in expressing tagged XLG protein at adequate levels for such assessments (Ding et al., 2008). While competition between GPA1 and XLGs for  $G\beta\gamma$  could be a common theme, it is also possible that XLG- and GPA1-based heterotrimers modulate shared molecular signaling pathways. GPA1 interacts with GCR1, the only putative Arabidopsis G protein-coupled receptor based on sequence and structural homology (Plakidou-Dymock et al., 1998; Pandey and Assmann, 2004; Warpeha et al., 2007; Taddese et al., 2014), GTG1/GTG2, the two Arabidopsis G protein-coupled receptor-type G proteins (Pandey et al., 2009), and RGS1, the sole demonstrated  $G\alpha$  GTPase-activating protein in Arabidopsis (Chen et al., 2003). The potential interactions of the XLGs with these signaling elements remain to be explored.

#### Interaction of XLG Proteins with $G\beta\gamma$ Dimers in Vivo

The interaction of one of the XLGs, XLG2, with  $G\beta\gamma$  was shown by yeast three-hybrid analysis and confirmed by BiFC by Maruta et al. (2015), but interaction strength was not investigated. We now demonstrate that all three XLGs bind  $G\beta\gamma$  dimers, with distinct specificity, and with differences in binding strength in

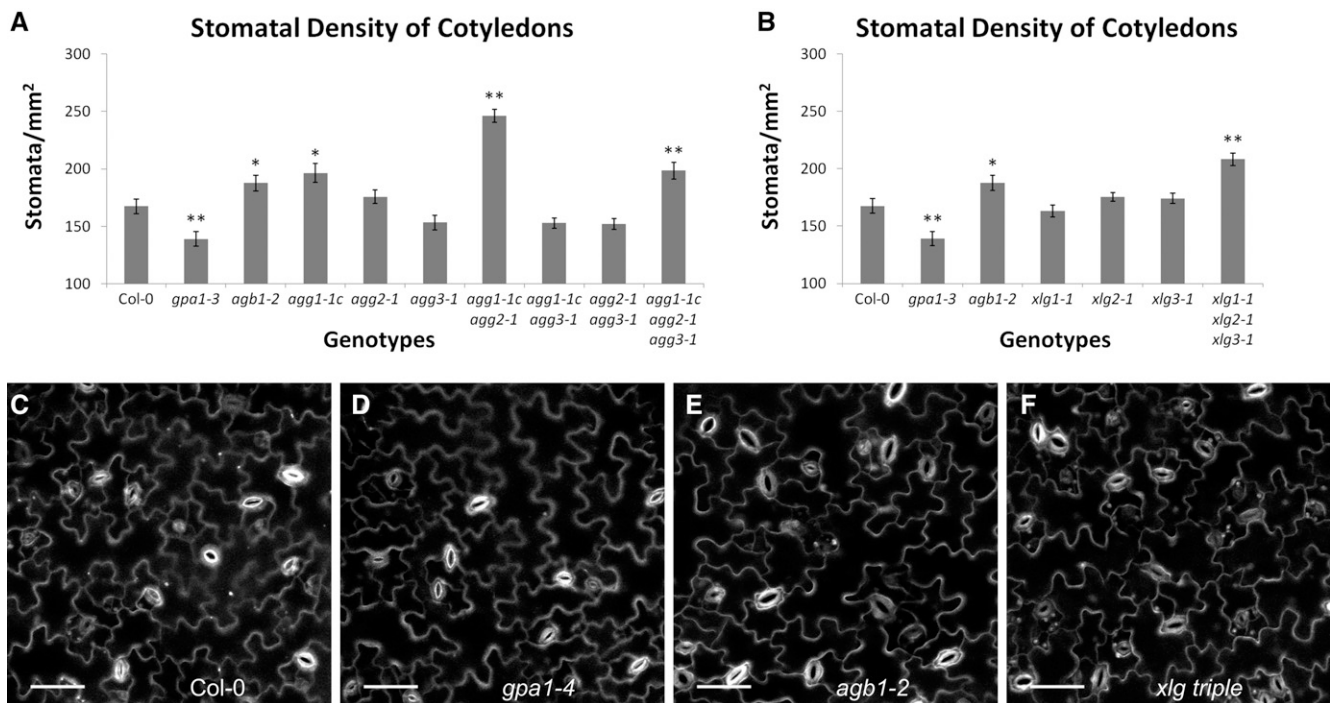


**Figure 14.** *agb1*, *agg1* *agg2*, and the *xlg* triple mutants display increased stomatal density. Propidium iodide-stained cotyledons of 9-d-old seedlings were imaged using a confocal microscope, and images were used to quantify stomatal density for mutants of the  $G\gamma$  subunits (A) and *xlg* mutants (B). The assay was conducted for all genotypes simultaneously, and the Col-0, *agb1-2*, and *gpa1-3* controls represent the same data in A and B. Significant differences from Col-0 (Student's *t* test) are indicated: \*,  $P < 0.05$  to 0.01; and \*\*,  $P < 0.01$  to 0.001. All values are means  $\pm$  s.e. Representative images of propidium iodide-stained cotyledons are shown for Col-0 (C), *gpa1-4* (D), *agb1-2* (E), and the *xlg* triple mutant (F). White indicates propidium iodide stain. Bars = 50  $\mu$ m.

the yeast three-hybrid system. The canonical  $G\alpha$  subunit, GPA1, displayed a preference for AGB1/AGG3( $\gamma$ ) over AGB1/AGG1 or AGB1/AGG2 (Fig. 1A). Similarly strong, or even stronger, interactions than that of GPA1 with AGB1/AGG3( $\gamma$ ) were observed for several of the XLG- $G\beta\gamma$  interactions (Fig. 1). The fact that XLG interactions with  $G\beta\gamma$  dimers are as strong as or stronger than the  $G\beta\gamma$  interactions of the canonical GPA1 is evidence that XLGs function in the heterotrimer.

There were some slight discrepancies between the yeast three-hybrid results of Maruta et al. (2015) and our yeast three-hybrid data. For example, Maruta et al. (2015) obtained positive results using XLG2, AGB1, and an untagged AGG3 subunit, whereas our results were negative using XLG2 and AGG3, with untagged AGB1 as the bridge protein (Fig. 1C). One explanation is that the XLG2-AGB1/AGG3 interaction is extremely weak and fell below the detectable threshold in our conditions and assay configuration. It also should be noted that negative yeast three-hybrid results are not always definitive for lack of interaction. For example, we did not see strong evidence for GPA1/AGB1/AGG1 or GPA1/AGB1/AGG2 heterotrimers in yeast, yet *gpa1*, *agb1*, and *agg1-1c agg2-1* mutants all display hypersensitivity to D-Glc repression of germination (Ullah et al., 2002; Pandey et al., 2006; Trusov et al., 2007), functionally implicating complexes of these subunits in

planta. As GPA1/AGB1/AGG1 and GPA1/AGB1/AGG2 heterotrimers have been observed in planta by BiFC (Gookin and Assmann, 2014), the formation of these heterotrimers likely requires plant-specific cofactors.

Maruta et al. (2015) previously showed that XLG2 interacted with all three Arabidopsis  $G\beta\gamma$  dimers by BiFC. However, the use of the sticky N-173/C-155 overlap-based split enhanced yellow fluorescent protein (eYFP) fragments (Kodama and Hu, 2012), coupled with strong expression driven by the double 35S promoter present in the pSAT vectors and a relatively long protoplast incubation time of 16 to 24 h, could confound the results (Maruta et al., 2015). To assess XLG- $G\beta\gamma$  heterotrimer formation, we performed BiFC for all three XLGs using the pDOE low-background BiFC system (Gookin and Assmann, 2014). Our results show that all three XLGs interact with AGB1/AGG1, AGB1/AGG2, and AGB1/AGG3 at the plasma membrane (Figs. 5 and 6), with a signal localization pattern reminiscent of the GPA1- $G\beta\gamma$  BiFC signal (Gookin and Assmann, 2014). Importantly, no BiFC signal was observed in the absence of a coexpressed  $G\gamma$  subunit, demonstrating, as in our yeast three-hybrid results, that the XLG- $G\beta$  interaction is not bipartite and that true heterotrimer formation occurs. This contrasts with the data from Maruta et al. (2015), which showed BiFC signal between XLG2 and the three  $G\gamma$  subunits in *agb1*

protoplasts. One possible explanation is that XLG2 and the  $G\gamma$  subunits exist in a complex strong and stable enough (without AGB1) to allow detectable BiFC. Alternatively, the BiFC signal observed by Maruta et al. (2015) could have arisen from nonspecific self-assembly of the BiFC fragments, as outlined above.

### XLG Localization

The previously described subcellular localization of XLGs in the nucleus and  $G\beta\gamma$  dimers at the plasma membrane could provide an impediment to the hypothesis that XLGs function as heterotrimeric G protein subunits, although AGB1 localization to the nucleus has also been reported, albeit without an equivalently expressed  $G\gamma$  subunit that might provide a membrane anchor for the  $G\beta\gamma$  dimer (Anderson and Botella, 2007). We reassessed the subcellular localization of the XLGs using *Agrobacterium tumefaciens*-mediated transient transformation in *N. benthamiana*, as opposed to biolistic expression in *Vicia faba* guard cells (Ding et al., 2008). Our assays indicate that the three XLGs have variable preferences for nuclear localization (Fig. 7; Supplemental Fig. S6). The extranuclear localization of all three proteins at the cell periphery is consistent with the recent report of XLG localization at the plasma membrane (Maruta et al., 2015). Our BiFC data show XLG heterotrimer localization is restricted to the cell periphery, specifically at the plasma membrane (Figs. 5 and 6). However, in BiFC, the two tagged interacting proteins are physically coupled by the irreversible association of the split fluoroprotein and are not free to move independently. Therefore, we examined the influence of untagged  $G\beta\gamma$  dimers on XLG localization, choosing XLG3:mVenus as an example, since it reliably showed nearly even localization in the cytosol and nucleus. When provided in excess, untagged AGB1/AGG1 or AGB1/AGG2 dimers were able to sequester XLG3 at the plasma membrane, in many cases rendering the nucleus devoid of XLG3 signal (Fig. 10). In the absence of cosupplied  $G\beta\gamma$ , the diverse localization patterns are also supported by our bioinformatic analysis and residue substitution mutants, which show that XLG2 has a noncanonical NLS (Fig. 8) and that XLG3 has both a classical NLS (Ding et al., 2008) and an unconventional NES (Fig. 9). It is intriguing to speculate that, upon activation and dissociation from  $G\beta\gamma$ , the XLGs may act to directly transfer signal from the plasma membrane to the nucleus. This idea is lent credence by the interaction of XLG with RELATED TO VERNALIZATION1 (RTV1), a DNA-binding protein with a plant-specific B3-like DNA-binding domain (Heo et al., 2012). RTV1 plays an important role in flowering time control, likely by regulating floral integrator genes such as *SUPPRESSOR OF OVEREXPRESSION OF CONSTANS1* and *FLOWERING LOCUS T*. The XLG2-RTV1 interaction occurs in the nucleus and stimulates RTV1 chromatin binding in chromatin immunoprecipitation assays (Heo et al., 2012).

### XLGs Function in G Protein-Related Phenotypes

If XLGs function with  $G\beta\gamma$  dimers in a  $G\alpha$ -like manner, XLG mutation should result in G protein-associated phenotypes. Some indicators that XLGs participate in AGB1 signaling are known (Table I). Based on the analysis of G protein phenotypes in the literature, we identified four other *agb1* phenotypes in which *gpa1* mutants behaved like the wild type, displayed an opposite phenotype to *agb1*, or had not been assigned. Salt, tunicamycin, and D-Glc are abiotic stresses that *agb1* mutants are hypersensitive to during postgermination development. In the absence of similar phenotypes in *gpa1* mutants, we examined the *xlg* mutants and identified *agb1*-like phenotypes in the *xlg* triple mutant (Figs. 11–14). Our results thereby indicate that XLG1,2,3/AGB1/AGG1,2 heterotrimers play a role in suppressing responses to abiotic stress. Salt has recently been implicated in stimulation of the UPR (Liu and Howell, 2010; Wang et al., 2011), much as tunicamycin traditionally has been. Therefore, G proteins can be hypothesized to function as suppressors of the UPR downstream of the convergence of different stimuli such as salt and tunicamycin. Similarly, AGB1, AGG1 and AGG2, but not GPA1, have been implicated in cell death and ROS production downstream of receptor-like kinases such as BAK1-INTERACTING RECEPTOR-LIKE KINASE1 (BIR1), FLAGELLIN-SENSITIVE2, EF-Tu RECEPTOR, and CHITIN ELICITOR RECEPTOR KINASE1 (Liu et al., 2013). Additionally, Respiratory burst oxidase protein D- and F-mediated *P. syringae* resistance and ROS production are dependent on AGB1 but not GPA1 (Torres et al., 2013), and an increased rate of powdery mildew entry into epidermal cells was observed upon surface inoculation of *agb1* but not *gpa1* mutant leaves (Lorek et al., 2013). Indeed, Maruta et al. (2015) demonstrated that disruption of either XLG2 or AGB1 was able to suppress the cell death phenotype of *bir1* and resulted in impaired pathogen defense responses, including ROS production. These results illustrate that G proteins modulate multiple cell death pathways, either suppressing (Warpeha et al., 2008; Wei et al., 2008; Chen and Brandizzi, 2012; Colaneri et al., 2014; Yu and Assmann, 2015) or stimulating (Liu et al., 2013; Maruta et al., 2015) cell death in a stimulus-specific manner. XLGs also function in developmental pathways. *xlg* mutants display increased primary root growth (Ding et al., 2008) and increased root waving and skewing (Pandey et al., 2008), both of which are also *agb1* phenotypes (Chen et al., 2006; Pandey et al., 2008). We demonstrate that XLGs are also involved in the development of aerial tissues, with *xlg* mutants exhibiting an increase in stomatal density (Fig. 14).

The subunit phenotypes, including those summarized in Table I and those we analyzed in Figures 11 to 14, correlate well with the heterotrimer configurations we observed in yeast (Fig. 1). We found significant overlap of *agg1* and *agg2* phenotypes with *xlg* phenotypes. With the exception of hypersensitivity to D-Glc during germination (Pandey et al., 2006; Trusov et al.,

2007), few overlapping phenotypes between *gpa1* and *agg1/agg2* mutants have been identified to date. This observation, in combination with our yeast data, suggests that there are eight higher affinity heterotrimer combinations that are responsible for the majority of G protein signaling: GPA1/AGB1/AGG3, XLG1/AGB1/AGG1, XLG1/AGB1/AGG2, XLG2/AGB1/AGG1, XLG2/AGB1/AGG2, XLG3/AGB1/AGG1, XLG3/AGB1/AGG2, and XLG3/AGB1/AGG3. Our criteria for choosing potential *xlg* phenotypes to investigate centered on *agg1* and/or *agg2* phenotypes that were not recapitulated in *gpa1* mutants. Therefore, it should be noted that our study was deliberately biased toward the investigation of potential *xlg/agb1/agg1-agg2* phenotypes and was not expected to identify additional *gpa1/agb1/agg1-agg2* phenotypes.

The distinct phenotypes displayed by *gpa1* and *xlg* mutants suggest that GPA1 and the XLGs mediate distinct molecular pathways, at least in some cases, and that competition between GPA1 and the XLGs for  $G\beta\gamma$  binding could be important for molecular function. Additionally, GPA1 and the XLGs would be expected to bind and regulate different sets of effectors. A small number of GPA1 interactors have been described that could be evaluated for interaction with XLGs, including PHOSPHOLIPASE  $D\alpha 1$  (Zhao and Wang, 2004), PREPHENATE DEHYDRATASE1 (Warpeha et al., 2006), PIRIN1 (Warpeha et al., 2007; Orozco-Nunnally et al., 2014), THYLAKOID FORMATION1 (Huang et al., 2006), and those identified in the interactome of Klopffleisch et al. (2011). There may also be effector specificity within the XLG family, as the majority of the G protein-related pathogen responses have been attributed to XLG2 (Zhu et al., 2009; Maruta et al., 2015). However, significant overlap among XLG effectors is also expected, due to the redundancy displayed by the XLGs in our salinity (Fig. 11), tunicamycin (Fig. 12), D-Glc (Fig. 13), and stomatal density (Fig. 14) assays.

### Extending G Protein Heterotrimer Diversity

The lack of G protein diversity in plants such as *Arabidopsis* has been an unexpected finding in the post-genomic era. The initial identification of GPA1, AGB1 ( $G\beta$ ), and AGG1/AGG2 ( $G\gamma$ ) allowed for only two different heterotrimer combinations, which was assumed from 2001 to 2011 to be the full complement of *Arabidopsis* G protein subunits, until the identification of the atypical  $G\gamma$  subunit, AGG3 (Chakravorty et al., 2011). Even the characterization of AGG3 only expanded the number of heterotrimer combinations to three and, surprisingly, suggested that  $G\gamma$  was the only subunit conferring isoform diversity in *Arabidopsis*. Here, we provide evidence from several complementary approaches that all three XLGs function as components of the heterotrimeric G protein complex. XLGs and GPA1 bind selected  $G\beta\gamma$  dimers with similar or greater strength (Fig. 1), and XLG3 and GPA1 compete with each other for the binding of AGB1/AGG3 in our yeast results

(Fig. 3). Furthermore, in silico analysis suggests that the three XLG proteins structurally resemble GPA1 (Fig. 4; Supplemental Figs. S1 and S2; Supplemental Tables S1 and S2). All three XLGs interact with  $G\beta\gamma$  dimers in planta (Fig. 5), XLG3 is sequestered at the plasma membrane by both AGB1/AGG1 and AGB1/AGG2 (Fig. 10), and *xlg* triple mutants phenocopy several *agb1* phenotypes (Figs. 11–14). Therefore, it appears that the  $G\alpha$  family in *Arabidopsis* comprises four members: GPA1, XLG1, XLG2, and XLG3. The addition of the XLGs as  $G\alpha$  subunits expands the repertoire of heterotrimer combinations from three to 12.

## MATERIALS AND METHODS

### Plant Lines and Growth Conditions

All *Arabidopsis* (*Arabidopsis thaliana*) transfer DNA insertions used have been described previously and were isolated in the Col-0 background, with the exception of *agg1-1c*, which was identified in the Wassilewskija ecotype but introgressed into Col-0 by Trusov et al. (2007). Mutants used were *gpa1-3* and *gpa1-4* (Jones et al., 2003), *agb1-2* (Ullah et al., 2003), *xlg1-1*, *xlg2-1*, *xlg3-1*, and the *xlg1-1 xlg2-1 xlg3-1* triple mutant (Ding et al., 2008), *agg1-1c* and *agg2-1* (Trusov et al., 2007), and *agg3-1* (Chakravorty et al., 2011). Aside from the *agg1-1c agg2-1* double mutant (Trusov et al., 2007), the  $G\gamma$  double and triple mutants have not previously been described but are combinations of the above published alleles. *Arabidopsis* plants were grown in Metro Mix 360 soil (Sun Gro Horticulture), and *Nicotiana benthamiana* plants were grown in a 1:1 mix of Metro Mix 360 and Sunshine Mix LC1 (Sun Gro Horticulture), in growth chambers with an 8-h-light/16-h-dark cycle, 120  $\mu\text{mol photons m}^{-2} \text{s}^{-1}$  light, and 20°C.

### Yeast Three-Hybrid Experiments

XLG clones were mobilized from pCR8/GW/TOPO (Life Technologies) into pDEST-GADT7 (Uetz et al., 2006) by Gateway cloning methods (Life Technologies).  $G\gamma$  subunit genes and truncations of the  $G\gamma$  subunits were cloned into the *EcoRI/SalI* restriction sites of MCS1 of pBridge. AGB1 was cloned into the *NotI/BglIII* restriction sites of MCS2 to generate yeast (*Saccharomyces cerevisiae*) three-hybrid constructs that express the  $G\beta$  and  $G\gamma$  subunits. Competition assay constructs were made by cloning XLG3 or GPA1 into the *SpeI/EcoRI* sites of p416GPD under the control of the strong yeast promoter GPD. The GPDpr::XLG3::CYC1 terminator and GPDpr::GPA1::CYC1 terminator expression cassettes were excised from the vectors by PCR, which added flanking *NotI* and *BspEI* restriction sites. The PCR fragments were cloned into the *NotI/BspEI* sites in the backbone of pDEST-GADT7-GPA1 and pDEST-GADT7-XLG3 vectors, yielding pDEST-GADT7-GPA1-GPDpr::XLG3 and pDEST-GADT7-XLG3-GPDpr::GPA1 vectors, respectively, for competition assays.

Yeast assays were performed in the Y2HGold yeast strain background (Clontech). Diploid cells from mating of Y2HGold bait strains with Y187 (Clontech) prey strains were selected on SC-Trp-Leu plates. To test for the presence and strength of interactions, diploid cells were spotted onto SC-Trp-Leu-Met-His medium supplemented with a range of 3-AT concentrations (0, 1, 2, 5, 10, 20, and 30 mM) to suppress His synthesis at increasing 3-AT levels (Durfee et al., 1993). Interaction was assessed by activation of the His synthesis reporter gene, which was scored by yeast growth, and the strength of interaction was assessed by growth on plates supplemented with progressively higher 3-AT concentrations.

### BiFC and Fluorescent Protein Analyses

BiFC and localization analysis was performed essentially as described previously (Gookin and Assmann, 2014). Protocols for agroinfiltration, protoplast transformation, and confocal microscopy, as well as a description of the improved pDOE vector set used here, can be found in a recent publication (Gookin and Assmann, 2014). Cloning was performed using the strategies outlined in detail by Gookin and Assmann (2014), Methods S1 and S2. Briefly, XLGL protein fusions with internal NVen210 fragments were created by overlap PCR and inserted into the pDOE-10 MCS1 (simultaneously removing

the vector-encoded tag) to create parent vectors. AGB1 was inserted into MCS3 to create the three UBIQUITIN10 promoter-driven XLGL-CVEN210:AGB1 test vectors. UBIQUITIN10-driven XLG and residue-substituted XLG:mVenus fusions were created similarly by bridging pDOE-17 MCS1 and MCS3 in one cloning step (i.e. the 5' end of the open reading frame was cloned into MCS1 and the 3' end into MCS3). Likewise, the mTq2:histone 2B construct was created by bridging MCS1 and MCS3 of pDOE-19. The 35S promoter-driven untagged AGB1-AGG and single AGG constructs were made similarly and utilized previously (Gookin and Assmann, 2014). Agroinfiltration at low optical densities is critical for avoiding artifacts; therefore, test vectors were infiltrated at a final OD<sub>600</sub> of 0.0075 to 0.01. When utilized, additional subunits were added in presumed excess by infiltrating at an OD<sub>600</sub> of 0.025 to 0.03. The FM4-64 dye (Life Technologies), which marks the plasma membrane, was diluted to 50  $\mu\text{M}$  and infiltrated into the transiently transformed *N. benthamiana* leaves just prior to imaging. Population level images were acquired at 20 $\times$  magnification. Finer detail images were collected using a 40 $\times$  magnification water-immersion objective. High-resolution/magnification images showing the specificity of histone 2B and XLG colocalization, and the specific overlap of XLG-G $\beta\gamma$  heterotrimer formation with the plasma membrane marker dye FM4-64, were obtained using a 63 $\times$  oil-immersion lens and a 1.1- $\mu\text{m}$  optical slice. The specific localization of XLG-G $\beta\gamma$  heterotrimer formation at the plasma membrane was further demonstrated at 95 $\times$  magnification by the additional application of a 1.5 $\times$  zoom of the confocal scan area during image acquisition (0.09  $\mu\text{m}$  per pixel resolution). Images were acquired using the Zeiss LSM-510 confocal microscope and analyzed using the Zen 2009/2012 software.

## Plate Assays

Plate assays were performed on standard 0.5 $\times$  MS medium (Sigma) plates with 1% (w/v) agar (Sigma) supplemented with 1% (w/v) Suc (Calbiochem) for all assays except the D-Glc sensitivity assay. After plating, seeds were stratified at 4°C for 2 d before plates were transferred to short-day growth chamber conditions, as described above. Assays were performed with plates oriented horizontally. In the salt sensitivity assay, seeds were plated as described above and grown for 9 d, and then the seedlings were transferred to medium supplemented with 150 mM NaCl (EMD Millipore). Seedlings were grown for an additional 14 to 21 d. Tunicamycin assays were performed similarly to the assay of Wang et al. (2006). Briefly, seeds were initially plated on medium supplemented with 0.15  $\mu\text{M}$  tunicamycin (Sigma). Seedlings were grown for 6 d, transferred to standard medium, and allowed to recover for an additional 10 d before scoring. Seedlings fell into three categories in our scoring system: (1) seedlings that did not grow after transfer from the tunicamycin plates and were clearly chlorotic and brown (dead); (2) seedlings that grew and often greened after transfer but were visibly impaired in their growth (stunted); and (3) seedlings that thrived after transfer (healthy). D-Glc sensitivity assays were performed using medium supplemented with 1% or 6% (w/v) D-Glc (Sigma) instead of Suc, with seedlings grown under a long-day 16-h-light/8-h-dark cycle. Seeds were germinated under high-light conditions (120  $\mu\text{mol photons m}^{-2} \text{s}^{-1}$ ) for 1 d before lights were dimmed to 60  $\mu\text{mol photons m}^{-2} \text{s}^{-1}$  as per the method of Wang et al. (2006), who described their assay as run under dim light. Seedlings were grown for 24 d. All plate assays were repeated at least three times with similar results.

## Stomatal Density Assay

Seeds were plated and stratified as above. Seedlings were grown horizontally for 9 d in growth chambers with an 8-h-light/16-h-dark cycle, 90 to 100  $\mu\text{mol photons m}^{-2} \text{s}^{-1}$  light, and 20°C. Cotyledons were excised, stained with 1.5  $\mu\text{M}$  propidium iodide (Sigma) for 30 min in the dark, and mounted on coverslips with the abaxial side facing down. Images of abaxial epidermes were taken using an inverted Zeiss LSM-510 confocal microscope with a 20 $\times$  objective lens. At least 10 seedlings were used for each genotype. Stomatal density was quantified from the images.

## Anthocyanin Extraction

Anthocyanins were extracted according to the method of Mancinelli et al. (1991) with minor modifications. Briefly, intact aerial tissue of three to five seedlings was weighed, placed in acidic methanol (1% [v/v] HCl), and stored at 4°C in the dark overnight. Absorbance of the buffer with the leached pigments was measured in duplicate at  $A_{530}$  and  $A_{657}$  for three independent samples per genotype per condition using a Nanodrop 2000 (Thermo Scientific). The peak absorbance of anthocyanins occurs at 530 nm; however, chlorophyll also absorbs light at 530 nm, at approximately 25% of its peak  $A_{657}$ . Therefore, as per

the procedure of Mancinelli et al. (1991), comparative anthocyanin content was estimated by calculating ( $A_{530} - 0.25 \times A_{657}$ ) per mg of aerial tissue.

Arabidopsis Genome Initiative (AGI) locus identifiers for the heterotrimeric G protein subunits outlined in this article are: GPA1 (AT2G26300), XLG1 (AT2G23460), XLG2 (AT4G34390), XLG3 (AT1G31930), AGB1 (AT4G34460), AGG1 (AT3G63420), AGG2 (AT3G22942), AGG3 (AT5G20635), and RGS1 (AT3G26090).

## Supplemental Data

The following supplemental materials are available.

**Supplemental Figure S1.** Predicted secondary structure elements of the G $\alpha$  regions of the XLGs.

**Supplemental Figure S2.** Rotated view of the predicted XLG3 structure in Figure 4.

**Supplemental Figure S3.** ProSA validation of the XLG3 G $\alpha$  theoretical structure model.

**Supplemental Figure S4.** ERRAT analysis of the XLG3 G $\alpha$  theoretical structure model.

**Supplemental Figure S5.** Population level images of XLG-AGB1 BiFC.

**Supplemental Figure S6.** High-magnification colocalization of XLGs and histone 2B.

**Supplemental Table S1.** Summary of structural template matches for the XLG proteins, obtained using Phyre<sup>2</sup>.

**Supplemental Table S2.** Summary of structural template matches for the XLG proteins, obtained using genTHREADER.

**Supplemental File S1.** Protein Data Bank file of the computationally derived XLG3 $\alpha$  structure.

Received February 17, 2015; accepted July 6, 2015; published July 8, 2015.

## LITERATURE CITED

- Anderson DJ, Botella JR (2007) Expression analysis and subcellular localization of the *Arabidopsis thaliana* G-protein  $\beta$ -subunit AGB1. *Plant Cell Rep* 26: 1469–1480
- Birnbaumer L (2007) Expansion of signal transduction by G proteins: the second 15 years or so. From 3 to 16  $\alpha$  subunits plus  $\beta\gamma$  dimers. *Biochim Biophys Acta* 1768: 772–793
- Bisht NC, Jez JM, Pandey S (2011) An elaborate heterotrimeric G-protein family from soybean expands the diversity of plant G-protein networks. *New Phytol* 190: 35–48
- Bitter GA, Egan KM (1984) Expression of heterologous genes in *Saccharomyces cerevisiae* from vectors utilizing the glyceraldehyde-3-phosphate dehydrogenase gene promoter. *Gene* 32: 263–274
- Bolte S, Talbot C, Boutte Y, Catrice O, Read ND, Satiat-Jeuemaitre B (2004) FM-dyes as experimental probes for dissecting vesicle trafficking in living plant cells. *J Microsc* 214: 159–173
- Bommert P, Je BI, Goldshmidt A, Jackson D (2013) The maize G $\alpha$  gene COMPACT PLANT2 functions in CLAVATA signalling to control shoot meristem size. *Nature* 502: 555–558
- Botella JR (2012) Can heterotrimeric G proteins help to feed the world? *Trends Plant Sci* 17: 563–568
- Botto JF, Ibarra S, Jones AM (2009) The heterotrimeric G-protein complex modulates light sensitivity in *Arabidopsis thaliana* seed germination. *Photochem Photobiol* 85: 949–954
- Bradford W, Buckholz A, Morton J, Price C, Jones AM, Urano D (2013) Eukaryotic G protein signaling evolved to require G protein-coupled receptors for activation. *Sci Signal* 6: ra37
- Chakravorty D, Trusov Y, Zhang W, Acharya BR, Sheahan MB, McCurdy DW, Assmann SM, Botella JR (2011) An atypical heterotrimeric G-protein  $\gamma$ -subunit is involved in guard cell K<sup>+</sup>-channel regulation and morphological development in *Arabidopsis thaliana*. *Plant J* 67: 840–851



- Chen JG, Gao Y, Jones AM (2006) Differential roles of Arabidopsis heterotrimeric G-protein subunits in modulating cell division in roots. *Plant Physiol* **141**: 887–897
- Chen JG, Jones AM (2004) AtRGS1 function in *Arabidopsis thaliana*. *Methods Enzymol* **389**: 338–350
- Chen JG, Willard FS, Huang J, Liang J, Chasse SA, Jones AM, Siderovski DP (2003) A seven-transmembrane RGS protein that modulates plant cell proliferation. *Science* **301**: 1728–1731
- Chen Y, Brandizzi F (2012) AtIRE1A/AtIRE1B and AGB1 independently control two essential unfolded protein response pathways in Arabidopsis. *Plant J* **69**: 266–277
- Cheng Z, Li JF, Niu Y, Zhang XC, Woody OZ, Xiong Y, Djonovic S, Millet Y, Bush J, McConkey BJ, et al (2015) Pathogen-secreted proteases activate a novel plant immune pathway. *Nature* **521**: 213–216
- Choudhury SR, Bisht NC, Thompson R, Todorov O, Pandey S (2011) Conventional and novel G $\gamma$  protein families constitute the heterotrimeric G-protein signaling network in soybean. *PLoS ONE* **6**: e23361
- Colaneri AC, Tunc-Ozdemir M, Huang JP, Jones AM (2014) Growth attenuation under saline stress is mediated by the heterotrimeric G protein complex. *BMC Plant Biol* **14**: 129
- Colovos C, Yeates TO (1993) Verification of protein structures: patterns of nonbonded atomic interactions. *Protein Sci* **2**: 1511–1519
- Coursol S, Fan LM, Le Stunff H, Spiegel S, Gilroy S, Assmann SM (2003) Sphingolipid signalling in *Arabidopsis* guard cells involves heterotrimeric G proteins. *Nature* **423**: 651–654
- Delgado-Cerezo M, Sánchez-Rodríguez C, Escudero V, Miedes E, Fernández PV, Jordá L, Hernández-Blanco C, Sánchez-Vallet A, Bednarek P, Schulze-Lefert P, et al (2012) Arabidopsis heterotrimeric G-protein regulates cell wall defense and resistance to necrotrophic fungi. *Mol Plant* **5**: 98–114
- Ding L, Pandey S, Assmann SM (2008) Arabidopsis extra-large G proteins (XLGs) regulate root morphogenesis. *Plant J* **53**: 248–263
- Durfee T, Becherer K, Chen PL, Yeh SH, Yang Y, Kilburn AE, Lee WH, Elledge SJ (1993) The retinoblastoma protein associates with the protein phosphatase type 1 catalytic subunit. *Genes Dev* **7**: 555–569
- Eisenberg D, Luthy R, Bowie JU (1997) VERIFY3D: assessment of protein models with three-dimensional profiles. *Methods Enzymol* **277**: 396–404
- Fan LM, Zhang W, Chen JG, Taylor JP, Jones AM, Assmann SM (2008) Abscisic acid regulation of guard-cell K<sup>+</sup> and anion channels in G $\beta$ - and RGS-deficient *Arabidopsis* lines. *Proc Natl Acad Sci USA* **105**: 8476–8481
- Gookin TE, Assmann SM (2014) Significant reduction of BiFC non-specific assembly facilitates *in planta* assessment of heterotrimeric G-protein interactors. *Plant J* **80**: 553–567
- Heidstra R, Welch D, Scheres B (2004) Mosaic analyses using marked activation and deletion clones dissect *Arabidopsis* SCARECROW action in asymmetric cell division. *Genes Dev* **18**: 1964–1969
- Heo JB, Sung S, Assmann SM (2012) Ca<sup>2+</sup>-dependent GTPase, extra-large G protein 2 (XLG2), promotes activation of DNA-binding protein related to vernalization 1 (RTV1), leading to activation of floral integrator genes and early flowering in *Arabidopsis*. *J Biol Chem* **287**: 8242–8253
- Huang J, Taylor JP, Chen JG, Uhrig JF, Schnell DJ, Nakagawa T, Korth KL, Jones AM (2006) The plastid protein THYLAKOID FORMATION1 and the plasma membrane G-protein GPA1 interact in a novel sugar-signaling mechanism in *Arabidopsis*. *Plant Cell* **18**: 1226–1238
- Hurowitz EH, Melnyk JM, Chen YJ, Kouros-Mehr H, Simon MI, Shizuya H (2000) Genomic characterization of the human heterotrimeric G protein  $\alpha$ ,  $\beta$ , and  $\gamma$  subunit genes. *DNA Res* **7**: 111–120
- Ishida T, Tabata R, Yamada M, Aida M, Mitsumasu K, Fujiwara M, Yamaguchi K, Shigenobu S, Higuchi M, Tsuji H, et al (2014) Heterotrimeric G proteins control stem cell proliferation through CLAVATA signaling in *Arabidopsis*. *EMBO Rep* **15**: 1202–1209
- Ishikawa A, Iwasaki Y, Asahi T (1996) Molecular cloning and characterization of a cDNA for the  $\beta$  subunit of a G protein from rice. *Plant Cell Physiol* **37**: 223–228
- Ishikawa A, Tsubouchi H, Iwasaki Y, Asahi T (1995) Molecular cloning and characterization of a cDNA for the  $\alpha$  subunit of a G protein from rice. *Plant Cell Physiol* **36**: 353–359
- Johnston CA, Taylor JP, Gao Y, Kimple AJ, Grigston JC, Chen JG, Siderovski DP, Jones AM, Willard FS (2007) GTPase acceleration as the rate-limiting step in *Arabidopsis* G protein-coupled sugar signaling. *Proc Natl Acad Sci USA* **104**: 17317–17322
- Johnston CA, Willard MD, Kimple AJ, Siderovski DP, Willard FS (2008) A sweet cycle for Arabidopsis G-proteins: recent discoveries and controversies in plant G-protein signal transduction. *Plant Signal Behav* **3**: 1067–1076
- Jones AM, Ecker JR, Chen JG (2003) A reevaluation of the role of the heterotrimeric G protein in coupling light responses in Arabidopsis. *Plant Physiol* **131**: 1623–1627
- Jones DT (1999a) GenTHREADER: an efficient and reliable protein fold recognition method for genomic sequences. *J Mol Biol* **287**: 797–815
- Jones DT (1999b) Protein secondary structure prediction based on position-specific scoring matrices. *J Mol Biol* **292**: 195–202
- Jones JC, Duffy JW, Machius M, Temple BRS, Dohlman HG, Jones AM (2011a) The crystal structure of a self-activating G protein  $\alpha$  subunit reveals its distinct mechanism of signal initiation. *Sci Signal* **4**: ra8
- Jones JC, Temple BRS, Jones AM, Dohlman HG (2011b) Functional reconstitution of an atypical G protein heterotrimer and regulator of G protein signaling protein (RGS1) from *Arabidopsis thaliana*. *J Biol Chem* **286**: 13143–13150
- Kato C, Mizutani T, Tamaki H, Kumagai H, Kamiya T, Hirobe A, Fujisawa Y, Kato H, Iwasaki Y (2004) Characterization of heterotrimeric G protein complexes in rice plasma membrane. *Plant J* **38**: 320–331
- Kelley LA, Sternberg MJE (2009) Protein structure prediction on the Web: a case study using the Phyre server. *Nat Protoc* **4**: 363–371
- Kloppfleisch K, Phan N, Augustin K, Bayne RS, Booker KS, Botella JR, Carpita NC, Carr T, Chen JG, Cooke TR, et al (2011) Arabidopsis G-protein interactome reveals connections to cell wall carbohydrates and morphogenesis. *Mol Syst Biol* **7**: 532
- Kodama Y, Hu CD (2012) Bimolecular fluorescence complementation (BiFC): a 5-year update and future perspectives. *Biotechniques* **53**: 285–298
- Koizumi N, Martinez IM, Kimata Y, Kohno K, Sano H, Chrispeels MJ (2001) Molecular characterization of two Arabidopsis Ire1 homologs, endoplasmic reticulum-located transmembrane protein kinases. *Plant Physiol* **127**: 949–962
- Kosugi S, Hasebe M, Matsumura N, Takashima H, Miyamoto-Sato E, Tomita M, Yanagawa H (2009) Six classes of nuclear localization signals specific to different binding grooves of importin  $\alpha$ . *J Biol Chem* **284**: 478–485
- Kosugi S, Hasebe M, Tomita M, Yanagawa H (2008) Nuclear export signal consensus sequences defined using a localization-based yeast selection system. *Traffic* **9**: 2053–2062
- la Cour T, Kierner L, Mølgaard A, Gupta R, Skriver K, Brunak S (2004) Analysis and prediction of leucine-rich nuclear export signals. *Protein Eng Des Sel* **17**: 527–536
- Lease KA, Wen J, Li J, Doke JT, Liscum E, Walker JC (2001) A mutant *Arabidopsis* heterotrimeric G-protein  $\beta$  subunit affects leaf, flower, and fruit development. *Plant Cell* **13**: 2631–2641
- Lee YRJ, Assmann SM (1999) *Arabidopsis thaliana* 'extra-large GTP-binding protein' (AtXLG1): a new class of G-protein. *Plant Mol Biol* **40**: 55–64
- Li S, Liu Y, Zheng L, Chen L, Li N, Corke F, Lu Y, Fu X, Zhu Z, Bevan MW, et al (2012) The plant-specific G protein  $\gamma$  subunit AGG3 influences organ size and shape in *Arabidopsis thaliana*. *New Phytol* **194**: 690–703
- Liu J, Ding P, Sun T, Nitta Y, Dong O, Huang X, Yang W, Li X, Botella JR, Zhang Y (2013) Heterotrimeric G proteins serve as a converging point in plant defense signaling activated by multiple receptor-like kinases. *Plant Physiol* **161**: 2146–2158
- Liu JX, Howell SH (2010) Endoplasmic reticulum protein quality control and its relationship to environmental stress responses in plants. *Plant Cell* **22**: 2930–2942
- Llorente F, Alonso-Blanco C, Sánchez-Rodríguez C, Jorda L, Molina A (2005) ERECTA receptor-like kinase and heterotrimeric G protein from Arabidopsis are required for resistance to the necrotrophic fungus *Plectosphaerella cucumerina*. *Plant J* **43**: 165–180
- Lorek J, Griebel T, Jones AM, Kuhn H, Panstruga R (2013) The role of Arabidopsis heterotrimeric G-protein subunits in MLO2 function and MAMP-triggered immunity. *Mol Plant Microbe Interact* **26**: 991–1003
- Ma H, Yanofsky MF, Meyerowitz EM (1990) Molecular cloning and characterization of *GPA1*, a G protein  $\alpha$  subunit gene from *Arabidopsis thaliana*. *Proc Natl Acad Sci USA* **87**: 3821–3825
- Mancinelli AL, Rossi F, Moroni A (1991) Cryptochrome, phytochrome, and anthocyanin production. *Plant Physiol* **96**: 1079–1085
- Maruta N, Trusov Y, Brenya E, Parekh U, Botella JR (2015) Membrane-localized extra-large G proteins and G $\beta\gamma$  of the heterotrimeric G proteins form functional complexes engaged in plant immunity in Arabidopsis. *Plant Physiol* **167**: 1004–1016
- Mason MG, Botella JR (2000) Completing the heterotrimer: isolation and characterization of an *Arabidopsis thaliana* G protein  $\gamma$ -subunit cDNA. *Proc Natl Acad Sci USA* **97**: 14784–14788

- Mason MG, Botella JR (2001) Isolation of a novel G-protein  $\gamma$ -subunit from *Arabidopsis thaliana* and its interaction with G $\beta$ . *Biochim Biophys Acta* 1520: 147–153
- McCudden CR, Hains MD, Kimple RJ, Siderovski DP, Willard FS (2005) G-protein signaling: back to the future. *Cell Mol Life Sci* 62: 551–577
- Nilson SE, Assmann SM (2010) The  $\alpha$ -subunit of the *Arabidopsis* heterotrimeric G protein, GPA1, is a regulator of transpiration efficiency. *Plant Physiol* 152: 2067–2077
- Ohashi K, Kiuchi T, Shoji K, Sampei K, Mizuno K (2012) Visualization of cofilin-actin and Ras-Raf interactions by bimolecular fluorescence complementation assays using a new pair of split Venus fragments. *Bio-techniques* 52: 45–50
- Oldham WM, Hamm HE (2008) Heterotrimeric G protein activation by G-protein-coupled receptors. *Nat Rev Mol Cell Biol* 9: 60–71
- Orozco-Nunnelly DA, Muhammad D, Mezzich R, Lee BS, Jayathilaka L, Kaufman LS, Warpeha KM (2014) Pirin1 (PRN1) is a multifunctional protein that regulates quercetin, and impacts specific light and UV responses in the seed-to-seedling transition of *Arabidopsis thaliana*. *PLoS ONE* 9: e93371
- Pandey S, Assmann SM (2004) The *Arabidopsis* putative G protein-coupled receptor GCR1 interacts with the G protein  $\alpha$  subunit GPA1 and regulates abscisic acid signaling. *Plant Cell* 16: 1616–1632
- Pandey S, Chen JG, Jones AM, Assmann SM (2006) G-protein complex mutants are hypersensitive to abscisic acid regulation of germination and postgermination development. *Plant Physiol* 141: 243–256
- Pandey S, Monshausen GB, Ding L, Assmann SM (2008) Regulation of root-wave response by extra large and conventional G proteins in *Arabidopsis thaliana*. *Plant J* 55: 311–322
- Pandey S, Nelson DC, Assmann SM (2009) Two novel GPCR-type G proteins are abscisic acid receptors in *Arabidopsis*. *Cell* 136: 136–148
- Partow S, Siewers V, Bjørn S, Nielsen J, Maury J (2010) Characterization of different promoters for designing a new expression vector in *Saccharomyces cerevisiae*. *Yeast* 27: 955–964
- Plakidou-Dymock S, Dymock D, Hooley R (1998) A higher plant seven-transmembrane receptor that influences sensitivity to cytokinins. *Curr Biol* 8: 315–324
- Schröder M, Kaufman RJ (2005) ER stress and the unfolded protein response. *Mutat Res* 569: 29–63
- Taddese B, Upton GJG, Bailey GR, Jordan SRD, Abdulla NY, Reeves PJ, Reynolds CA (2014) Do plants contain G protein-coupled receptors? *Plant Physiol* 164: 287–307
- Thung L, Chakravorty D, Trusov Y, Jones AM, Botella JR (2013) Signaling specificity provided by the *Arabidopsis thaliana* heterotrimeric G-protein  $\gamma$  subunits AGG1 and AGG2 is partially but not exclusively provided through transcriptional regulation. *PLoS ONE* 8: e58503
- Thung L, Trusov Y, Chakravorty D, Botella JR (2012)  $G\gamma 1 + G\gamma 2 + G\gamma 3 = G\beta$ : the search for heterotrimeric G-protein  $\gamma$  subunits in *Arabidopsis* is over. *J Plant Physiol* 169: 542–545
- Torres MA, Morales J, Sánchez-Rodríguez C, Molina A, Dangi JL (2013) Functional interplay between *Arabidopsis* NADPH oxidases and heterotrimeric G protein. *Mol Plant Microbe Interact* 26: 686–694
- Trusov Y, Rookes JE, Chakravorty D, Armour D, Schenk PM, Botella JR (2006) Heterotrimeric G proteins facilitate *Arabidopsis* resistance to necrotrophic pathogens and are involved in jasmonate signaling. *Plant Physiol* 140: 210–220
- Trusov Y, Rookes JE, Tilbrook K, Chakravorty D, Mason MG, Anderson D, Chen JG, Jones AM, Botella JR (2007) Heterotrimeric G protein  $\gamma$  subunits provide functional selectivity in G $\beta\gamma$  dimer signaling in *Arabidopsis*. *Plant Cell* 19: 1235–1250
- Trusov Y, Zhang W, Assmann SM, Botella JR (2008)  $G\gamma 1 + G\gamma 2 \neq G\beta$ : heterotrimeric G protein  $G\gamma$ -deficient mutants do not recapitulate all phenotypes of G $\beta$ -deficient mutants. *Plant Physiol* 147: 636–649
- Uetz P, Dong YA, Zeretzke C, Atzler C, Baiker A, Berger B, Rajagopala SV, Roupelieva M, Rose D, Fossum E, et al (2006) Herpesviral protein networks and their interaction with the human proteome. *Science* 311: 239–242
- Ullah H, Chen JG, Temple B, Boyes DC, Alonso JM, Davis KR, Ecker JR, Jones AM (2003) The  $\beta$ -subunit of the *Arabidopsis* G protein negatively regulates auxin-induced cell division and affects multiple developmental processes. *Plant Cell* 15: 393–409
- Ullah H, Chen JG, Wang S, Jones AM (2002) Role of a heterotrimeric G protein in regulation of *Arabidopsis* seed germination. *Plant Physiol* 129: 897–907
- Ullah H, Chen JG, Young JC, Im KH, Sussman MR, Jones AM (2001) Modulation of cell proliferation by heterotrimeric G protein in *Arabidopsis*. *Science* 292: 2066–2069
- Urano D, Colaneri A, Jones AM (2014) G $\alpha$  modulates salt-induced cellular senescence and cell division in rice and maize. *J Exp Bot* 65: 6553–6561
- Urano D, Jones JC, Wang H, Matthews M, Bradford W, Bennetzen JL, Jones AM (2012a) G protein activation without a GEF in the plant kingdom. *PLoS Genet* 8: e1002756
- Urano D, Phan N, Jones JC, Yang J, Huang J, Grigston J, Taylor JP, Jones AM (2012b) Endocytosis of the seven-transmembrane RGS1 protein activates G-protein-coupled signalling in *Arabidopsis*. *Nat Cell Biol* 14: 1079–1088
- Ursic D, Chinchilla K, Finkel JS, Culbertson MR (2004) Multiple protein/protein and protein/RNA interactions suggest roles for yeast DNA/RNA helicase Sen1p in transcription, transcription-coupled DNA repair and RNA processing. *Nucleic Acids Res* 32: 2441–2452
- Wall MA, Posner BA, Sprang SR (1998) Structural basis of activity and subunit recognition in G protein heterotrimers. *Structure* 6: 1169–1183
- Wang HX, Weerasinghe RR, Perdue TD, Cakmakci NG, Taylor JP, Marzluff WF, Jones AM (2006) A Golgi-localized hexose transporter is involved in heterotrimeric G protein-mediated early development in *Arabidopsis*. *Mol Biol Cell* 17: 4257–4269
- Wang M, Xu Q, Yuan M (2011) The unfolded protein response induced by salt stress in *Arabidopsis*. *Methods Enzymol* 489: 319–328
- Wang S, Narendra S, Fedoroff N (2007) Heterotrimeric G protein signaling in the *Arabidopsis* unfolded protein response. *Proc Natl Acad Sci USA* 104: 3817–3822
- Wang XQ, Ullah H, Jones AM, Assmann SM (2001) G protein regulation of ion channels and abscisic acid signaling in *Arabidopsis* guard cells. *Science* 292: 2070–2072
- Warpeha KM, Gibbons J, Carol A, Slusser J, Tree R, Durham W, Kaufman LS (2008) Adequate phenylalanine synthesis mediated by G protein is critical for protection from UV radiation damage in young etiolated *Arabidopsis thaliana* seedlings. *Plant Cell Environ* 31: 1756–1770
- Warpeha KM, Lateef SS, Lapić Y, Anderson M, Lee BS, Kaufman LS (2006) G-protein-coupled receptor 1, G-protein G $\alpha$ -subunit 1, and prephenate dehydratase 1 are required for blue light-induced production of phenylalanine in etiolated *Arabidopsis*. *Plant Physiol* 140: 844–855
- Warpeha KM, Upadhyay S, Yeh J, Adamiak J, Hawkins SI, Lapić YR, Anderson MB, Kaufman LS (2007) The GCR1, GPA1, PRN1, NF-Y signal chain mediates both blue light and abscisic acid responses in *Arabidopsis*. *Plant Physiol* 143: 1590–1600
- Wei Q, Zhou W, Hu G, Wei J, Yang H, Huang J (2008) Heterotrimeric G-protein is involved in phytochrome A-mediated cell death of *Arabidopsis* hypocotyls. *Cell Res* 18: 949–960
- Weiss CA, Garnaat CW, Mukai K, Hu Y, Ma H (1994) Isolation of cDNAs encoding guanine nucleotide-binding protein  $\beta$ -subunit homologues from maize (ZGB1) and *Arabidopsis* (AGB1). *Proc Natl Acad Sci USA* 91: 9554–9558
- Wiederstein M, Sippl MJ (2007) ProSA-web: interactive web service for the recognition of errors in three-dimensional structures of proteins. *Nucleic Acids Res* 35: W407–W410
- Wolfenstetter S, Chakravorty D, Kula R, Urano D, Trusov Y, Sheahan MB, McCurdy DW, Assmann SM, Jones AM, Botella JR (2015) Evidence for an unusual transmembrane configuration of AGG3, a class C G $\gamma$  subunit of *Arabidopsis*. *Plant J* 81: 388–398
- Xu D, Grishin NV, Chook YM (2012) NESdb: a database of NES-containing CRM1 cargoes. *Mol Biol Cell* 23: 3673–3676
- Yachdav G, Kloppmann E, Kajan L, Hecht M, Goldberg T, Hamp T, Hönigschmid P, Schafferhans A, Roos M, Bernhofer M, et al (2014) PredictProtein: an open resource for online prediction of protein structural and functional features. *Nucleic Acids Res* 42: W337–W343
- Yu Y, Assmann SM (May 12, 2015) The heterotrimeric G-protein  $\beta$  subunit, AGB1, plays multiple roles in the *Arabidopsis* salinity response. *Plant Cell Environ* <http://dx.doi.org/10.1111/pce.12542>
- Zhang L, Hu G, Cheng Y, Huang J (2008) Heterotrimeric G protein  $\alpha$  and  $\beta$  subunits antagonistically modulate stomatal density in *Arabidopsis thaliana*. *Dev Biol* 324: 68–75
- Zhao J, Wang X (2004) *Arabidopsis* phospholipase D $\alpha 1$  interacts with the heterotrimeric G-protein  $\alpha$ -subunit through a motif analogous to the DRY motif in G-protein-coupled receptors. *J Biol Chem* 279: 1794–1800
- Zhu H, Li GJ, Ding L, Cui X, Berg H, Assmann SM, Xia Y (2009) *Arabidopsis* extra large G-protein 2 (XLG2) interacts with the G $\beta$  subunit of heterotrimeric G protein and functions in disease resistance. *Mol Plant* 2: 513–525